R. & M. No. 2533
(7604)
A.R.C. Technical Report

MINISTRY OF SUPPLY

AERONAUTICAL RESEARCH COUNCIL
REPORTS AND MEMORANDA

An Experimental Investigation of the Effect of Localised Masses on the Flutter of a Model Wing

By

N. C. LAMBOURNE, B.Sc. and D. WESTON, B.Sc.
of the Aerodynamics Division, N.P.L.

LONDON: HIS MAJESTY'S STATIONERY OFFICE
1951
PRICE 5*s* 6*d* NET

An Experimental Investigation of the Effect of Localised Masses on the Flutter of a Model Wing

By

N. C. LAMBOURNE, B.Sc. and D. WESTON, B.Sc.

of the Aerodynamics Division, N.P.L.

Reports and Memoranda No. 2533

12*th April*, 1944

Summary.—This report contains an account of some experiments on the effect of concentrated masses (representing wing engines, etc.) on the flutter characteristics of a model cantilever wing. Flutter critical speeds and frequencies were measured for an extensive range of mass loading and the results are presented in the form of diagrams. The flutter motions for a few representative conditions of mass loading were determined by an analysis of cinematograph pictures. The results of experiments on the influence of the flexibility of an engine mounting are also included.

1. *Introduction.*—The work described in this report was undertaken partly to indicate the general tendencies in the changes of flutter critical speed and frequency that occur when concentrated masses are added to a wing, and partly to provide an experimental control on methods of critical speed prediction. A detailed theoretical investigation of the subject by Frazer is still proceeding, but his prelimary results[1,2] for a few representative mass conditions accord well with the corresponding experimental results of the present report. The experimental results also show qualitative agreement with calculations made by Minnhinick and Yarwood[3].

A further report will deal with the resonance and stiffness tests carried out in conjunction with the flutter experiments.

2. *Range of Investigation.*—Measurements of critical speed and frequency were made for an extensive range of mass-loading at each of the three sections 0·1, 0·3 and 0·5 span, and at chordwise positions as follows :—

(i) Forward of leading edge.

(ii) At 0·3 chord behind leading edge (*i.e.*, at approximately flexural axis).

(iii) Behind flexural axis.

Mass combinations at two or three positions were included, and a few cases of mass loading at the tip section were also investigated. The modes of deformation of the wing were measured for a few representative flutter conditions, and tests were also made to determine the influence of the flexibility of the engine support.

(92986) A

3. *Description of the Wing.*—The model tapered cantilever wing (Figs. 1, 2 and 3) apart from the detachable fittings representing wing engines, was similar to the wing specified in R. & M. 1782[4] and was designed to be representative of full-scale from the point of view of wing density, mass distribution (mass per unit span proportional to c^2), and stiffness distribution (linear taper of dimensions along the span). Its elastic stiffnesses were chosen so that the critical speed for flutter as estimated by the method of R. & M. 1782 for the bare wing (*i.e.*, without engine mass attachments), was about 90 ft/sec.

The transverse reference axis OY lay at $0{\cdot}3$ chord aft of the leading edge and the principal wing data were as follows :—

Span (root to tip) s	$= 6$ ft.
Root chord c_0	$= 2{\cdot}7$ ft.
Tip chord c_t	$= 1{\cdot}414$ ft.
Spanwise co ordinate η	$= y/s$.
Local chord c	$= c_0(1 - 10\eta/21)$.
*Flexural stiffness (measured at $\eta = 0{\cdot}7$) l_ϕ:	$= 1{,}790$ lb ft/rad.
*Torsional stiffness (measured at $\eta = 0{\cdot}7$) m_θ	$= 97{\cdot}8$ lb ft/rad.

Mean position of flexural axis $0{\cdot}32c$ behind leading edge.

Inertia axis (bare wing) $0{\cdot}4c$ behind leading edge.

Weight of bare wing $12{\cdot}7$ lb ($0{\cdot}394$ slug).

Wing density (bare wing) $0{\cdot}5$ lb/ft^3.

Radius of gyration about OY $0{\cdot}28c$.

The chordwise section was the symmetrical cubic oval $t/c = 0{\cdot}3898\ (1 - x/c)\sqrt{x/c}$, where t is the thickness.

The wing was constructed mainly of spruce. Its two equal spars of cruciform cross-section were firmly fixed into a root block, and were placed symmetrically with respect to OY in order to obtain a flexural axis at approximately $0{\cdot}3c$ behind the leading edge. To ensure fore-and-aft rigidity, the horizontal web of each spar was considerably stronger than the vertical one. The spars were cross-connected by thirty equally spaced ribs, the fixing being by small glued wooden fillets. Varnished paper glued on to the front spar formed the leading edge, whilst the trailing edge was a spruce lath.

For convenience in the application of loads to the wing in static deflection tests, small metal eyelets were attached to certain ribs ($\eta = 0{\cdot}1, 0{\cdot}2, 0{\cdot}3$, etc.) at the spar positions on both upper and lower surfaces. Local strengthening of the ribs around each eyelet was effected by means of plywood.

Throughout the tests the wing was supported horizontally with the root block firmly fixed, while ball-socket fittings were provided at sections $\eta = 0{\cdot}1$, $0{\cdot}3$ and $0{\cdot}5$ so that external springs could be attached to take up the deflections due to gravity. It was found, however, that supporting springs at two points in section $\eta = 0{\cdot}5$ were sufficient. Tests with the plane of the wing vertical would have avoided the use of external springs, but gravity stiffnesses would have been introduced and these would have varied with the additional masses.

During construction an inventory was kept of the masses and inertial constants of all the components of the wing† ; correction masses were then added to each rib as required to adjust the position of the inertia axis of the covered wing to $0{\cdot}1c$ aft of the reference axis. The wing density (excluding any engine mass attachments) was finally brought to $0{\cdot}5$ lb/cu ft by masses at ten positions along each spar. The various internal mass-loading positions were left accessible

* These were the initial values ; for fuller information *see* Table 1.

† A detailed specification of the mass properties of the wing will be included in a further report dealing with resonance and stiffness tests.

without disturbance of the main vaseline-doped silk covering by the use of small panels of silk carried by light frames attached to the appropriate ribs. Fig. 3 shows the covered wing with some of the panels removed.

Originally, provision was only made for the attachment of additional masses representing internal or external wing engines at three spanwise positions, $\eta = 0{\cdot}1$, $0{\cdot}3$ and $0{\cdot}5$. These " engine masses " consisted of lead castings weighing up to 10 lb and could be either fitted inside the wing at the reference axis to the specially strengthened ribs, or clamped securely to rigid bars (the engine mass mountings), which projected forward from the leading edge and were themselves bolted to the ribs. When external engine masses were present they were shielded by streamlined covers of tinplate to reduce disturbance of the air flow.

Subsequently mass loading was carried out at other positions in the wing. For this purpose the ball-socket fittings already mentioned were used together with other similar attachments, and the range of applied mass was greatly increased by an arrangement which is described in section 6.

For the flutter tests the wing was supported in a 9×7 ft wind-tunnel with the root block fixed to a massive steel pedestal. A " grab " which could be operated from outside the tunnel was arranged so that the tip section could be firmly held. As a further control on the wing motion it was possible by an electromagnetic device to apply friction to the wires connecting the mid-span section to the supporting springs. A combination of these two methods was usually sufficient to prevent the flutter getting out of control.

4. *Measurement of Critical Speeds and Frequencies.*—Critical speeds were measured by increasing the airspeed until a maintained oscillation resulted from an initial disturbance of the wing. The disturbance was effected either by a light cord attached to one of the supporting points in the mid-span section, or by allowing the wing to bounce between the jaws of the tip grab.

It was found that for the majority of mass-loading cases the airspeed needed very critical adjustment to ensure flutter of constant amplitude, and this critical speed was found to be sensibly independent of the intensity of the initial disturbance. In a few cases, notably in regions where the curve of critical speed with added mass was steep, it was found that maintained flutter would take place over a range of airspeeds, the amplitude increasing as the airspeed was raised. When this occurred the lowest speed at which a maintained oscillation could be detected was taken as the critical speed.

The critical speed for *spontaneous flutter* was also measured in some of the early tests. This was found to be approximately 10 ft/sec above the speed corresponding to the steady flutter already mentioned.

Flutter frequencies were originally measured by a chronograph operated by an electrical contact attached to the wing, but later when it became necessary to measure higher frequencies, a cathode-ray oscillograph was used instead of the chronograph.

Divergence speeds were determined by measuring the torsional stiffness at mid-span section for various airspeeds and extrapolating to find the speed corresponding to zero stiffness.

5. *Test Programme.*—The flutter tests were carried out in series, which are specified below, whilst the experiments with a flexible engine mounting are described in section 11.

Series I Mass loading at section $\eta = 0{\cdot}3$.
Series II Mass loading forward of leading edge.
Series III Mass loading at reference axis (*i.e.* $0{\cdot}3c$ behind leading edge).
Series IV Mass loading behind reference axis.
Series V Experiments with mass loading after the wing had been initially mass-balanced.

6. *Range of Mass Loading.*—Use was made of the lead masses described in section 3, but tests were also carried out with values of mass up to two slugs.* These abnormally large masses were applied indirectly by means of a lever fixed to the tunnel floor, carrying a weight and connected to the appropriate wing position by a wire. A supporting spring from above was attached to the same point in the wing. At frequency f the effective mass applied to the wing by the lever system was

$$m - \frac{\sigma}{4\pi^2 f^2},$$

where m is the equivalent mass of lever and weight, and σ is the stiffness of the supporting spring. The equivalent mass m was varied by altering the position of the weight along the lever. From the point of view of wing divergence the supporting spring acted as an additional elastic constraint; this explains why it was possible to measure flutter critical speeds above the divergence speed for the bare wing.

Two or three similar lever systems were used in experiments with mass-loading combinations.

Further tests were carried out with straining wires connected to the wing from above and below, so that a node occurred at the point of attachment. Statically this condition only represented an infinite elastic constraint, but with flutter it also corresponded to an infinite mass at that point.

For some cases with the rearward point locked, wing divergence was encountered.

Conditions corresponding to infinite mass provide information, such as the position of asymptotes and the presence of discontinuities in the critical speed curve, which is useful as a control on theoretical prediction.

7. *Application to Full-scale.*—Since the root of the model wing was supported rigidly, the mobility of the fuselage which is present on an actual aircraft was not represented. This mobility, and other neglected factors, will influence the critical speed in practice, so that the results of the model tests should not be relied upon for quantitative prediction of critical speeds of particular full-scale aircraft. Their main value is to indicate general tendencies.

The results for the model can, of course, be converted to refer to a dynamically similar full-scale wing, provided the two systems are assumed to be similarly supported. If L denotes a typical linear dimension, Σ a typical elastic stiffness (moment per radian), V_c the critical speed and f_c the critical frequency, then V_c^2 and f_c^2 vary respectively as ΣL^{-3} and ΣL^{-5}, while corresponding masses vary as L^3.

In the tests the mass loading was brought about either by means of lead weights or by effective masses located at points of the wing. Although a full-scale engine might justifiably be considered as a concentrated mass, it is not possible to represent a distributed load such as fuel in this manner. It is, however, relevant to state the values of the model masses that correspond to full-scale engines and fuel, and the following table, which is based on figures supplied by the Royal Aircraft Establishment, gives representative values of power plant and fuel weights, and the corresponding masses for the model.

	Power Plant		Fuel	
	Weight of power plants / Weight of bare wings	Corresponding model mass slug	Weight of fuel / Weight of bare wings	Corresponding model mass slug
Twin-engined fighter	2·5	0·99	1·5	0·59
Twin-engined bomber	1·6	0·63	2·1	0·83
Four-engined bomber	1·4	0·27 (per engine)	2·9	1·14

* In a few cases much higher values of mass loading were used.

8. *Change of Elastic Characteristics during the Tests.*—Unfortunately the wing was damaged at an early stage in the flutter tests owing to an unexpected divergence. A repair of the spars became necessary and this caused an increase in the wing stiffness. However, all the results recorded in this report were obtained after the accident occurred.

It was noticed during the resonance tests that the wing stiffness decreased with time, and this fact again became apparent as the flutter tests proceeded. Flutter frequencies were found to be lower when re-measured at a later date, although critical speed repeats were on the whole reasonably good. Table 1 gives values of wing stiffnesses measured at $\eta = 0{\cdot}7$, and critical speeds and frequencies for the bare wing as measured from time to time.

It is thought that this decrease of stiffness was due to the general weakening of the wing during the tests.

9. *Presentation of Results.*—The results are recorded in the form of diagrams, and in some cases the same results appear in more than one figure so that comparisons can easily be made.

Throughout, $\mu = \infty$ indicates that the loading point is fixed.

Series I. Mass Loading at Section $\eta = 0{\cdot}3$

Tests with combinations of masses,

μ_1 at $0{\cdot}28c$ ahead of leading edge ($x = -0{\cdot}58c$)

μ_2 at $0{\cdot}3c$ behind leading edge ($x = 0$)

μ_3 at $0{\cdot}69c$ behind leading edge ($x = +0{\cdot}39c$)

as shown below.

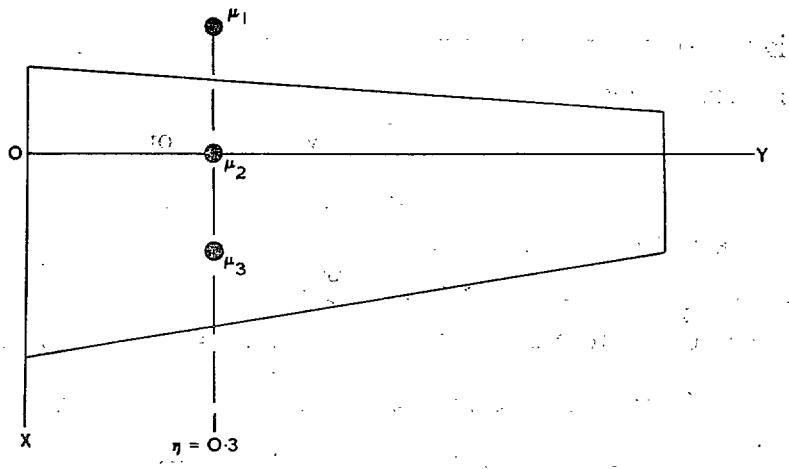

Results are shown in diagrams as follows.

With engine mounting in position

Figure	μ_1 slug	μ_2	μ_3
7	0	0 to ∞	0
8	0·157	0 to ∞	0
9	0·315	0 to ∞	0
10	∞	0 to ∞	0
11	0 to ∞	∞	0
12	0 to ∞	0	0
13	0	0	0 to ∞
14	0·157	0	0 to ∞
15	0·315	0	0 to ∞
16	∞	0	0 to ∞
17	0 to ∞	0	∞

Without engine mounting

Figure	μ_1	μ_2 slug	μ_3
18	0	0 to ∞	0
19	0	0 to ∞	∞
20	0	0	0 to ∞
21	0	0·312	0 to ∞
22	0	∞	0 to ∞

Series II. Mass Loading Forward of Leading Edge

Loading positions,

$\eta = 0{\cdot}1$ $0{\cdot}29c$ forward of leading edge ($x = -0{\cdot}59c$)
$\eta = 0{\cdot}3$ $0{\cdot}28c$ forward of leading edge ($x = -0{\cdot}58c$)
$\eta = 0{\cdot}5$ $0{\cdot}29c$ forward of leading edge ($x = -0{\cdot}59c$)

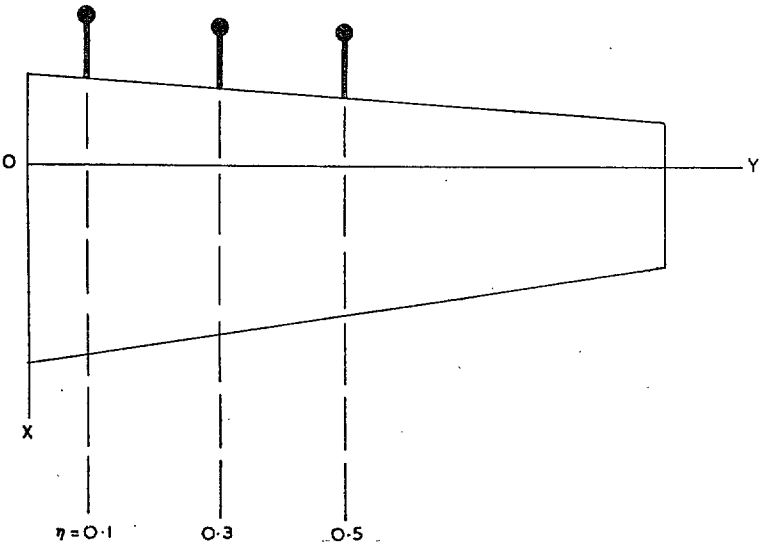

Mass μ was applied together with the appropriate engine mounting.

Fig. 23. Mass μ successively at

(i) $\eta = 0{\cdot}1$
(ii) $\eta = 0{\cdot}3$
(iii) $\eta = 0{\cdot}5$.

The difference between the three sets at $\mu = 0$ is due to the engine mountings.

Fig. 24. Equal masses μ simultaneously at $\eta = 0{\cdot}5, \eta = 0{\cdot}3$.

Fig. 25. Equal masses μ simultaneously at $\eta = 0{\cdot}5$, $\eta = 0{\cdot}3$, $\eta = 0{\cdot}1$.

Series III. Mass Loading at the Reference Axis

Loading positions,

$\eta = 0{\cdot}1$ $0{\cdot}3c$ behind leading edge.
$\eta = 0{\cdot}3$ $0{\cdot}3c$ behind leading edge.
$\eta = 0{\cdot}5$ $0{\cdot}3c$ behind leading edge.
$\eta = 1{\cdot}0$ $0{\cdot}3c$ behind leading edge.

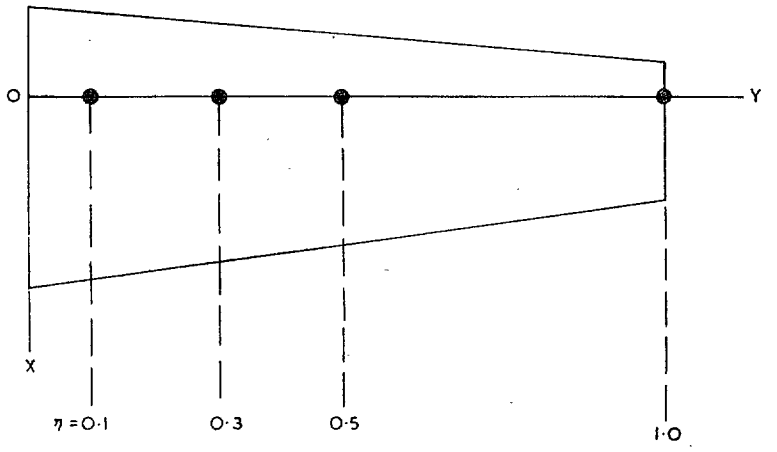

Fig. 26. Mass μ successively at

(i) $\eta = 0{\cdot}1$
(ii) $\eta = 0{\cdot}3$
(iii) $\eta = 0{\cdot}5$

Fig. 27. (i) Mass μ at $\eta = 0{\cdot}5$.
(ii) Equal masses μ simultaneously at $\eta = 0{\cdot}5$, $\eta = 0{\cdot}3$.

Fig. 28. (i) Mass μ at $\eta = 1{\cdot}0$.
(ii) Mass μ at $\eta = 1{\cdot}0$ simultaneously with $0{\cdot}155$ slug at $\eta = 0{\cdot}5$.
(iii) Mass μ at $\eta = 1{\cdot}0$ simultaneously with $0{\cdot}312$ slug at $\eta = 0{\cdot}5$.

Only small values of μ were used here, and a larger scale is convenient for the diagram.

Series IV. Mass Loading Behind Reference Axis

Loading positions,

$\eta = 0{\cdot}1$ $0{\cdot}65c$ behind leading edge ($x = 0{\cdot}35c$)
$\eta = 0{\cdot}3$ $0{\cdot}69c$ behind leading edge ($x = 0{\cdot}39c$)
$\eta = 0{\cdot}5$ $0{\cdot}74c$ behind leading edge ($x = 0{\cdot}44c$)

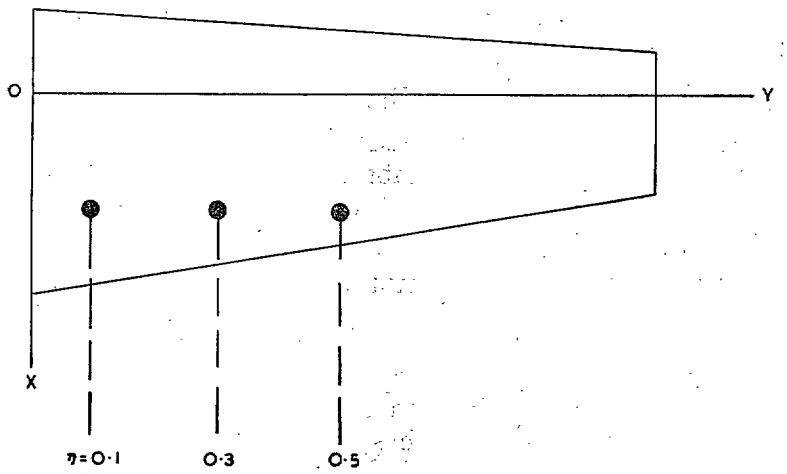

Fig. 29. Mass successively at

(i) $\eta = 0{\cdot}1$
(ii) $\eta = 0{\cdot}3$
(iii) $\eta = 0{\cdot}5$

Fig. 30. (i) μ at $\eta = 0{\cdot}5$.
(ii) Equal masses μ simultaneously at $\eta = 0{\cdot}5$, $\eta = 0{\cdot}3$.

Series V. Initially Mass-balanced Wing

The wing was assumed divided into ten spanwise segments and the centre of gravity of each segment was brought by means of lead weights to the reference axis (*i.e.*, $0{\cdot}3c$ behind leading edge). This modification also increased the wing density from $0{\cdot}5$ to $0{\cdot}55$ lb cu/ft.

With this new condition no flutter of the bare wing could be obtained although the airspeed was raised to just below the divergence speed.

It was at this stage that the divergence speed of the bare wing was measured and found to be 145 ft/sec.

(*a*) *Mass loading at* $\eta = 0{\cdot}3, 0{\cdot}28c$ *forward of leading edge.*—No flutter was obtained for airspeeds up to divergence although a number of mass values, including the ' wired up ' condition, were tried.

(*b*) *Mass loading at* $\eta = 0{\cdot}5, 0{\cdot}29c$ *forward of leading edge.*—(For simplicity the mass-balanced wing condition is denoted by $j = 0$, and the original condition by $j = 0{\cdot}1$).

Fig. 31. (i) $j = 0{\cdot}1$
(ii) $j = 0$

In this case critical speeds above the divergence speed for the bare wing were measured ; this has been explained in section 6.

(*c*) *Mass loading at reference axis* $\eta = 0{\cdot}3$.—No flutter obtained below divergence.

(*d*) *Mass loading at* $\eta = 0{\cdot}3, 0{\cdot}69c$ *behind leading edge.*

Fig. 32. (i) $j = 0{\cdot}1$
(ii) $j = 0$

10. *Flutter Modes.*—10·1 *Measurement.*—The wing was photographed from a window of the wind tunnel by a 16 mm ciné camera arranged at a height a little above the general level of the wing. Thus a foreshortened picture of the wing was obtained, showing both the leading and trailing edges ; these, together with the ribs at intervals 0·1 span, had been outlined with white paint. To provide a datum line for use in the analysis of the wing motion, two white crosses were marked on the tunnel wall near the wing root. A nominal film speed of 128 frames/sec was used, but an accurate time scale was given by including in the pictures a pointer which was rotated at 5 revs/sec by a small synchronous motor. An enlargement of a portion of one record is reproduced in Fig. 4.

Before the actual filming, the airspeed was carefully adjusted to give steady flutter.

For analysis, the film was projected frame by frame and measurements were obtained of the displacements at the spanwise stations defined by the intersection of the ribs and the leading and trailing edges. The position of each of these points was measured from a fixed datum line connecting the crosses. Measurements were made for a cycle of the wing motion, the frames being chosen to correspond approximately to intervals of 1/12 period.

Calibration factors were obtained by photography of scales placed at the various wing stations.

The motion of any wing section during a steady flutter oscillation may be written in the form of flexural and torsional components thus,

$$\phi = \Phi \sin (pt + \alpha),$$
$$\theta = \Theta \sin (pt + \beta),$$

where the flexure $\phi = z/s$ and the torsion θ are defined in Fig. 5.

The wing motion may conveniently be specified by the following.

Flexural component mode	$f(\eta) = \Phi/\Phi_t$
Torsional component mode	$F(\eta) = \Theta/\Theta_t$ (where suffix t refers to the tip section)
Flexural phase	$(\alpha - \alpha_t)$
Torsional phase	$(\beta - \alpha_t)$ (referred to the flexural component at the tip)
Amplitude ratio at tip	$(\Phi/\Theta)_t$

It should be noted that in this system $f(\eta)$ and $F(\eta)$ are amplitude modes and are necessarily positive.

Measurements from the film records were analysed on a 'Least Squares' basis to yield amplitudes and phases for each of the spanwise stations $\eta = 0{\cdot}3, 0{\cdot}4 \ldots 1{\cdot}0$*. The final results consist of the means of two analyses.

10·2. *Results.*—Analysis of the flutter motion was carried out for the following wing conditions.

A_0 bare wing

Mass-loading forward of leading edge at $\eta = 0{\cdot}3$ (*see* Fig. 12).

B_1 low frequency side of discontinuity (first branch),

B_2 high frequency side of discontinuity (second branch),

B_3 $\mu_1 = 0{\cdot}315$ slug (second branch).

Mass-loading on reference axis at $\eta = 0{\cdot}3$ (*see* Fig. 18).

A_1 low frequency side of discontinuity (first branch),

A_2 high frequency side of discontinuity (second branch).

The results are shown in Figs. 33 to 36, and a few points worthy of mention are set out below.

Bare wing.—Both the flexural and torsional modes approximate closely to curves $f(\eta) = F(\eta) = \eta^2$, and as no phase differences exist along the span the component motions can be described as simple.

Mass-loading forward of leading edge (*Figs.* 33 *and* 34).—(*a*) *First branch of critical speed curve.*—No change in amplitude modes, but there is a torsional phase difference along the span.

(*b*) *Second branch.*—Large phase differences occur, and the component modes are complex.

Mass-loading at reference axis. (*Figs.* 35 *and* 36).—(*a*) *First branch.*—No phase differences along the span, but there is a change in the amplitude modes.

(*b*) *Second branch.*—The component motions are complex, a large flexural phase change occurring along the span.

11. *Effect of Flexibility of Engine Mounting.*—11·1. *Full-scale Representation.*—Some experiments were carried out to find the effect of a flexible engine support on flutter characteristics. The important factors in this connection are, (i) the relation between the natural frequency of the engine on its support and the flutter frequency, and (ii) the damping present in the support. It is therefore important that the values of the natural frequency and damping of the model flexible support shall at least roughly correspond to those of full-scale practice.

Thus the frequency is determined by

$$\frac{f_0}{f_0'} = \frac{f}{f'} = \sqrt{\left\{\frac{\varepsilon}{\varepsilon'}\left(\frac{L'}{L}\right)^5\right\}},$$

where

f_0 is the natural frequency of the engine on its support,

f any other typical frequency of the wing,

ε a typical elastic stiffness (moment/angle),

L a typical dimension,

and the unaccented and accented symbols refer to model and full-scale respectively.

* It was found that measurement at sections $\eta = 0{\cdot}1$ and $0{\cdot}2$ was impracticable owing to low accuracy; also in some cases the projecting engine mounting obscured the leading-edge stations at these positions.

The damping relation is simply that the relative damping γ is the same for both model and full-scale. Relative damping is given by

$$\gamma = \frac{2\pi f_0 B}{C},$$

where

$B =$ damping coefficient of support (moment/angular velocity),

$C =$ stiffness of support (moment/angle).

The following figures for three aircraft with flexibly supported engines were quoted by the Royal Aircraft Establishment.

Aircraft	Pitching of Engine System	
	Frequency f_o' cycles/sec	Damping γ
a	7·9	0·03
b	13·3$_5$	0·09
c	8·5	0·08$_5$

Values of $\sqrt{\left\{\frac{\varepsilon}{\varepsilon'}\left(\frac{L'}{L}\right)^5\right\}}$ were obtained for a number of aircraft and found to lie within the range 0·3 to 0·8, so that if 10 cycles/sec. is taken to be the order of frequency for full-scale flexibly supported engines, the corresponding model frequency lies between 3 and 8 cycles/sec. It is significant that this range coincides roughly with the critical frequencies measured in the main flutter tests described in section 9. In the present tests the natural frequency of the engine system was varied within the range 4 to 11 cycles/sec., whilst the relative damping had approximate values $\gamma = 0{\cdot}1$ and $\gamma = 0{\cdot}3$.

11.2. *Apparatus and Tests.*—The mass-loading position forward of the leading edge at section $\eta = 0{\cdot}3$ was chosen, and the rigid mounting used in the previous tests was replaced by an arrangement shown diagrammatically in Fig. 6. F is a " Silentbloc " rubber bearing* and is fixed inside tube T which is rigidly attached to the wing. The rubber annulus of F together with springs S,S′ acts as a flexible support for rod R which carries engine mass M. The important degree of freedom from the point of view of these experiments is the ability of the rod and mass to perform a pitching oscillation about a virtual centre of rotation O. The natural frequency of oscillation of the mass about O is, for small angles, approximately

$$f_0 = \frac{1}{2\pi}\sqrt{\left\{\frac{\sigma + k/l^2}{m_0}\right\}},$$

where

σ is the combined stiffness of S and S′,

m_0 is the mass of M, assumed large compared with the mass of the rod,

k is the stiffness constant of the flexible bearing,

l is the distance between M and O.

It was possible to fix the bearing at one of two positions along the tube whilst mass M remained at a constant position with respect to the wing. That is, two values of l were possible so that two values C_1 and C_2 of the coupling stiffness could be used.

One reason for the choice of rubber as a flexible connection was that, since this medium is commonly used for full-scale engine mountings, the inherent damping obtained would be representative of full-scale. However, to increase the damping further the space between F and plug P could be packed with grease.

* This bearing consists of two concentric metal tubes with rubber compressed in the annular space.

The natural frequency and damping of the engine mass system were measured by separate resonance tests with m_0 varied. Tube T was rigidly clamped to a test-bed and a sinusoidal displacement was induced at the lower end of S′. The forced amplitude of M was measured for a range of forcing frequencies, and from the resulting amplitude-frequency curve the natural frequency and relative damping were found. The relative damping γ was given by the usual approximate formula $\gamma = (f_1 - f_2)/f_0$, where f_0 is the frequency for maximum amplitude (taken to be the natural frequency), and f_1, f_2 are frequencies corresponding to amplitudes $(1/\sqrt{2}) \times$ (maximum amplitude).

The results of the resonance tests are set out in Table 2.

Critical speeds and frequencies were measured for each of these masses, and also for other intermediate values. As a basis for comparison a corresponding set of critical speeds and frequencies was measured with a rigid mounting in which the rubber bearing has been replaced by a steel block of the same weight.

The results are plotted against $m \equiv (m_0 - \sigma/4\pi^2 f_c^2)$, where f_c is the flutter frequency and $\sigma/4\pi^2 f_c^2$ is the correction due to the presence of springs S S′. The natural frequency f_0 is a function of m_0 or alternatively is a function of m and f_c, and strictly it cannot be plotted against m. However, an approximate curve indicating the value of this quantity is also shown on the graphs.

In the Appendix it is shown that when damping is absent, a flexibly supported mass m is equivalent to a rigidly supported mass $\mu = m \frac{f_0^2}{f_0^2 - f_c^2}$. Hence for $f_c < f_0$ the presence of the flexibility in the support is effectively equivalent so far as concerns flutter, to an increase of the mass; whilst for $f_c > f_0$ the equivalent mass becomes negative, and may alternatively be considered as an elastic constraint to earth, of stiffness $4\pi^2 m \frac{f_c^2 f_0^2}{f_c^2 - f_0^2}$.

Fig. 37 refers to coupling stiffness C_1. In this case the flutter frequencies with the flexible mounting were below the natural frequencies. The dotted curve is deduced from the results with the rigid support, on the basis of the formula in the Appendix for the case of zero damping.

Fig. 38 gives the results for the lower coupling stiffness, C_2. The damping is sensibly the same as that appropriate to Fig. 37, but the range of natural frequencies now contains the flutter frequencies and the effect due to the flexibility is much more marked.

Fig. 39 was obtained again with stiffness C_2, but with the relative damping increased to approximately three times its original value. Comparison with Fig. 38 shows that the increase in damping does not affect the first branch, whilst comparison with Fig. 37 indicates that the damping has the same effect as increasing the stiffness.

Acknowledgment.—The writers wish to express their great indebtedness to the Photographic Section of the Physics Division, N.P.L. for the cinematography of the wing motion.

APPENDIX

Flexibly Supported Mass

(i) *Damping Absent.*—Consider the system shown in Fig. (a) which represents a mass m flexibly supported from point O of a wing by a spring of stiffness σ. Then if during an oscillation of the

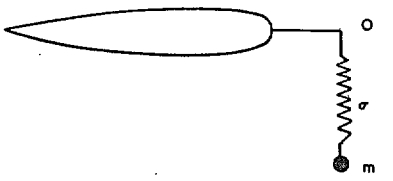

FIG. (a).

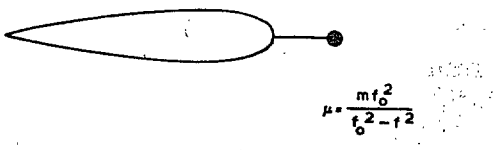

FIG. (b).

wing, O performs a motion which may sensibly be considered as simple harmonic in the vertical direction, the force at O is

$$-m\ddot{z}' = \sigma(z' - z) = -\mu\ddot{z}$$

where z and z' are the current displacements of O and m from their respective mean positions, and

$$\mu = \frac{\ddot{z}'}{\ddot{z}}\, m = \frac{mf_0^2}{f_0^2 - f^2},$$

where

f = frequency of oscillation

$f_0 = \frac{1}{2\pi}\sqrt{(\sigma/m)}$, the natural frequency of the $\overline{m,\ \sigma}$ combination.

Thus the system of Fig. (a) may be replaced by system Fig. (b) in which mass μ (which may be called the equivalent mass of $\overline{m,\ \sigma}$) is rigidly connected to the wing at O.

The variation μ/m with f/f_0 is shown in Fig. 40. It is seen that for values $f < f_0$, $\mu > m$ and when $f = f_0$, $\mu = \infty$ and for values $f > f_0$, μ is negative.

(ii) *Critical Speed and Frequency Prediction.*—Suppose that the variations of critical speed V_c, and critical frequency f_c, with rigidly connected mass μ are known, and are given in the form of diagrams of V_c and f_c plotted against μ. Then the flutter characteristics for a flexibly supported mass m, having natural frequency f_0 and negligible damping may be obtained by graphical solution of

$$\mu = \psi(f) = \frac{mf_0^2}{f_0^2 - f^2},$$

and

$$f_c = \phi(\mu),$$

the known variation of critical frequency with μ.

To obtain a finite mass scale it is convenient to plot f and f_c against tanh (μ/n) where n is chosen to give a suitable scale.

(iii) *Damping Present.*—Fig. (c) shows a similar mass-spring system, but in this case damping between the ends of the spring is included.

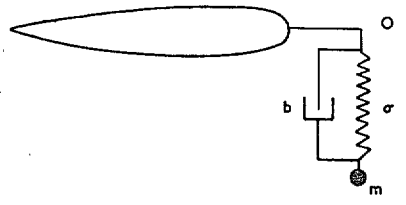

FIG. (c).

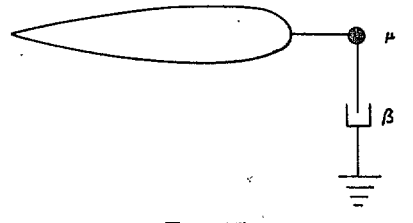

FIG. (d).

The force at O is now

$$-m\ddot{z}' = \sigma(z' - z) + b(\dot{z}' - \dot{z}) = -\mu\ddot{z} - \beta\dot{z},$$

where b is the damping coefficient and

$$\mu = m\frac{\sigma(\sigma - mp^2) + b^2p^2}{(\sigma - mp^2)^2 + b^2p^2},$$

$$\beta = \frac{m^2bp^4}{(\sigma - mp^2)^2 + b^2p^2},$$

$$p = 2\pi f.$$

Thus the system of Fig. (c) can be represented by a system as in Fig. (d), where mass μ is rigidly attached to the wing at point O, and damping β acts between O and earth.

Now if the damping between the ends of the spring in Fig. (c) is taken to obey Kussner's law of structural damping, *i.e.*,

$$\frac{bp}{\sigma} = \gamma \text{ (a constant)},$$

we may write

$$\frac{\mu}{m} = \frac{1 - (p/p_0)^2 + \gamma^2}{[1 - (p/p_0)^2]^2 + \gamma^2},$$

$$\frac{\beta}{pm} = \frac{\gamma(p/p_0)^2}{[1 - (p/p_0)^2]^2 + \gamma^2},$$

where

$$p_0 = \sqrt{(\sigma/m)}.$$

Figs. 40 and 41 shew the variations of μ/m and β/pm with $\frac{p}{p_0} \equiv \frac{f}{f_0}$.

REFERENCES

No.	*Author*	*Title, etc.*
1	R. A. Frazer	Interim Note on a Theoretical Investigation of the Influence of Mass on Wing Flutter. A.R.C. 6720. May, 1943. (Unpublished).
2	—	Addendum to above. A.R.C. 6833. June, 1943. (Unpublished).
3	I. T. Minhinnick and J. Yarwood ..	Interim Note on the Theoretical Effects of an Engine Mass on Wing Flutter. A.R.C. 6728. May, 1943. (To be published).
4	W. J. Duncan and H. M. Lyon ..	Calculated Flexural-Torsional Flutter Characteristics of some Typical Cantilever Wings. R. & M. 1782. April, 1937.

TABLE 1

Change of Elastic Characteristics of Wing

	Stiffnesses		Flutter Characteristics for bare wing	
	$l\varphi$ lb ft/rad	m_θ lb ft/rad	V_c ft/sec	f_c cycles/sec
March/April, 1942 (Standard flexibility coefficients.)	1790	97·8		
October, 1942 (Completion of preliminary resonance tests.)	1754	88·0		
December, 1942			86·1	5·45
January, 1943 (After repair to wing.)	1838	94·9	88·2	5·55
March, 1943			89·3 90·0	5·50 5·45
April, 1943			89·3 89·4	5·45 —
May, 1943			89·2	5·4
July, 1943			88·8 88·6	5·12 5·18
August, 1943	1550	85·3		

TABLE 2

Flexibly Supported Engine Mass — Natural Frequency and Damping

m_0	f_0	γ	
Stiffness C_1			
2·79 lb.	11·20 c.p.s.	0·12	
4·56	9·27	0·11	
6·52	8·05	0·12	0·11
8·84	6·87	0·11	
10·61	6·18	0·10	
Stiffness C_2			
2·79	7·62	0·10	
4·56	6·14	0·11	
6·52	5·13	0·10	0·10
8·84	4·42	0·10	
10·61	4·07	0·09	
Stiffness C_2 *with Added Damping*			
2·79	8·70	—	
4·56	6·74	0·35	
6·52	5·63	0·34	0·34
8·84	4·82	0·33	
10·61	4·41	0·35	

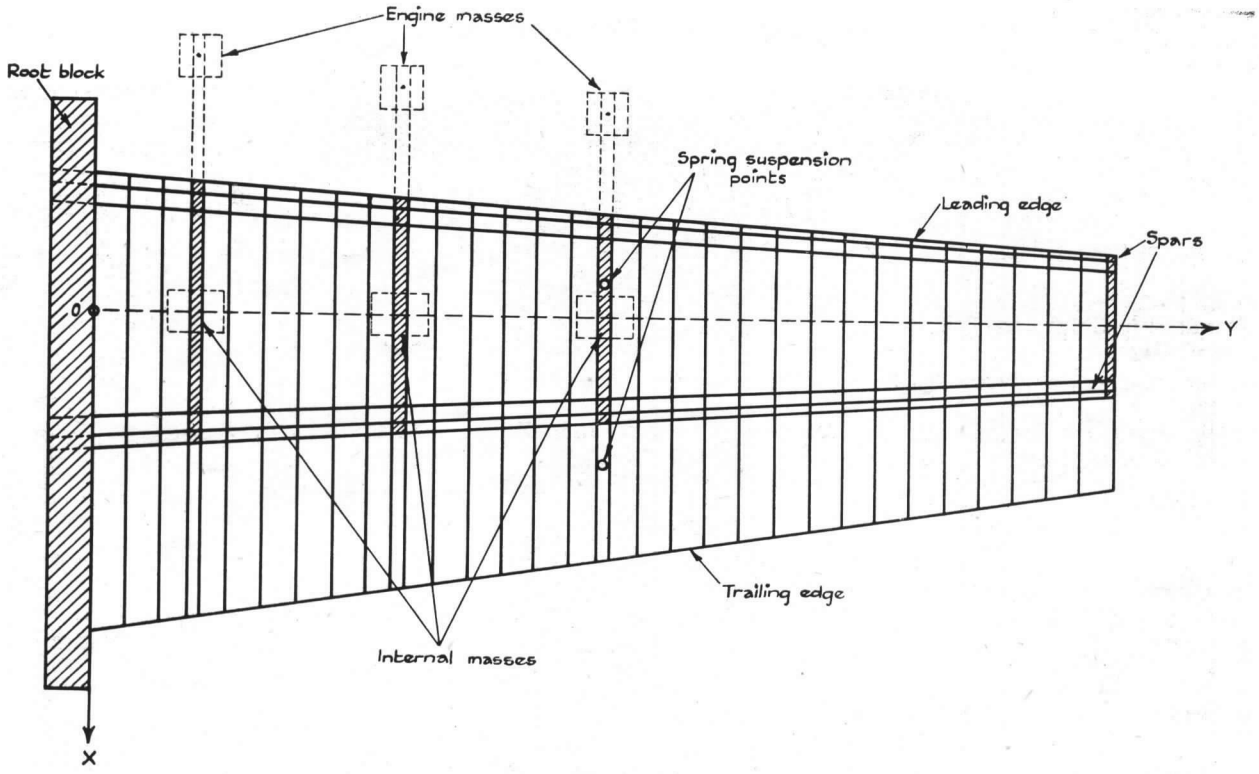

FIG. 1. Diagram of Wing.

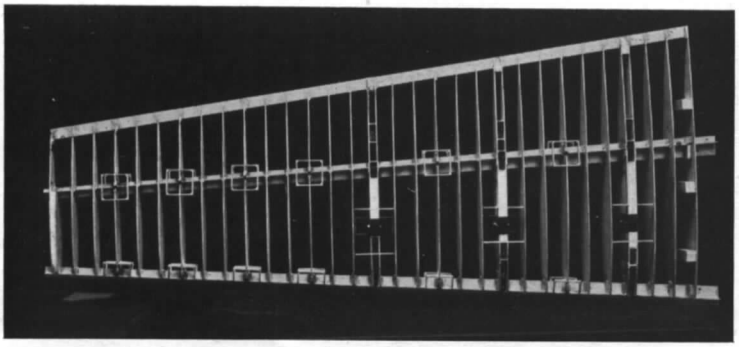

FIG. 2. Uncovered Wing.

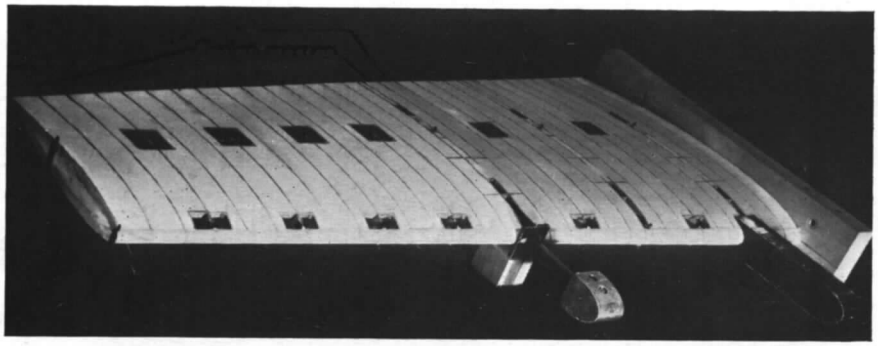

FIG. 3. Covered Wing showing Engine Masses.

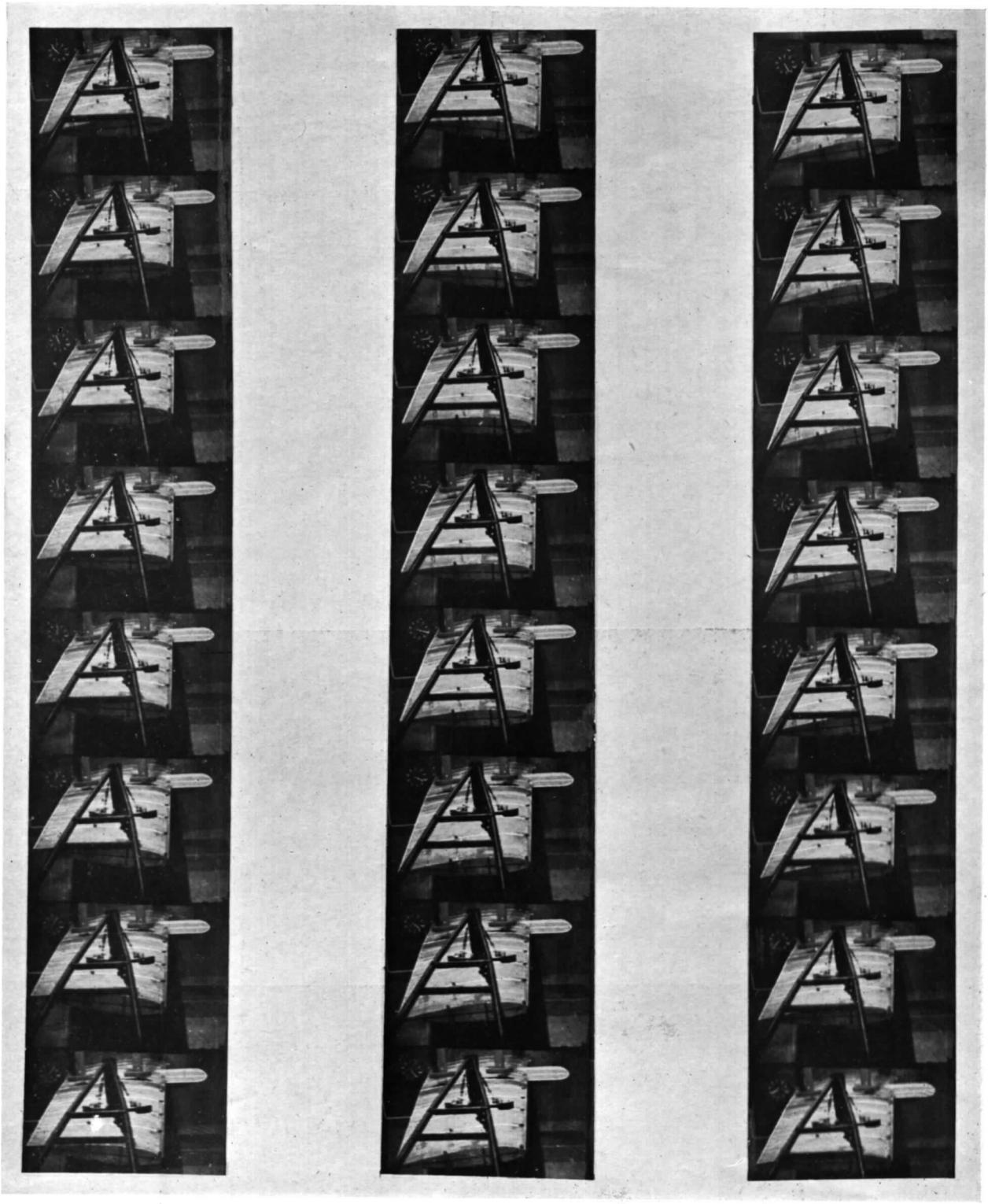

FIG. 4. Record of Flutter Motion.

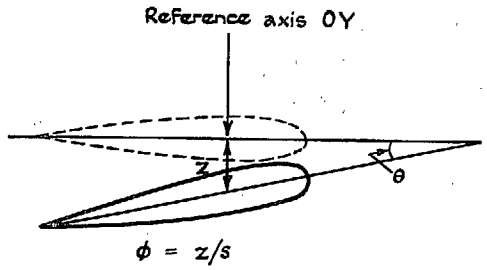

FIG. 5. Wing Motion Co-ordinates.

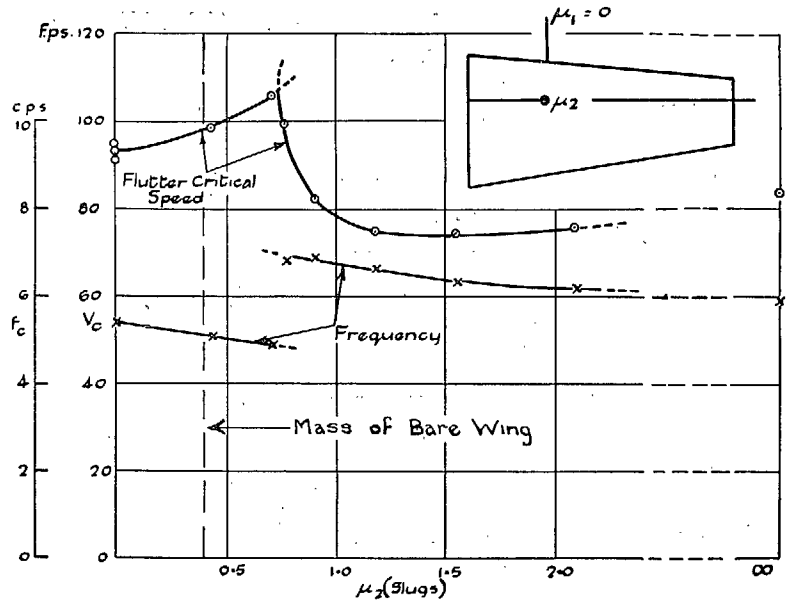

FIG. 7.

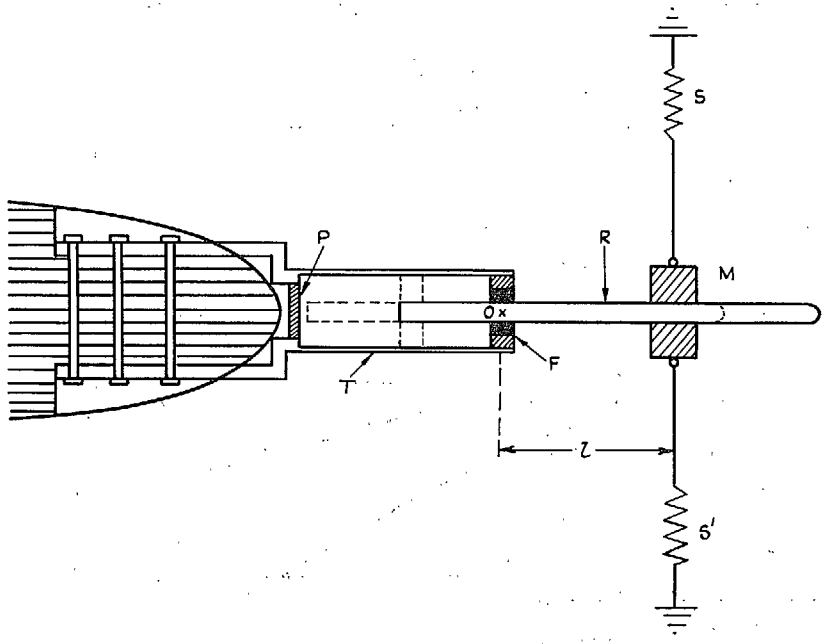

FIG. 6. Diagram of Flexible Engine Mounting.

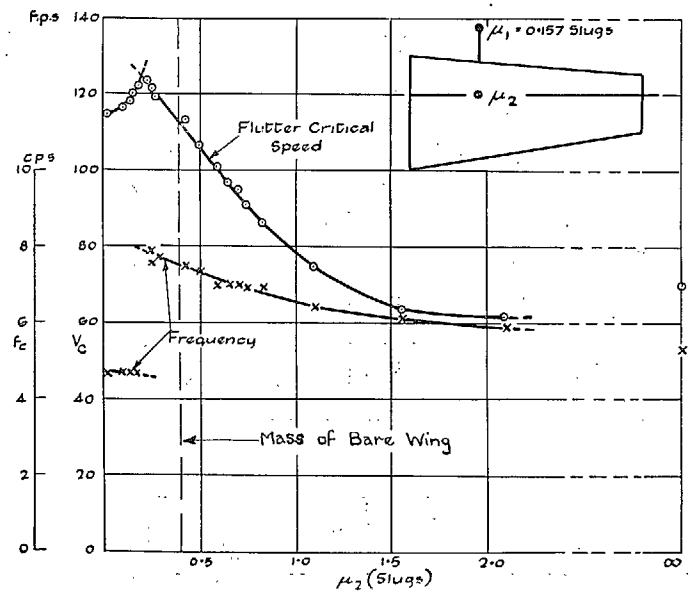

FIG. 8. Variation of Critical Speed and Frequency with Mass Loading at $\eta = 0{\cdot}3$.

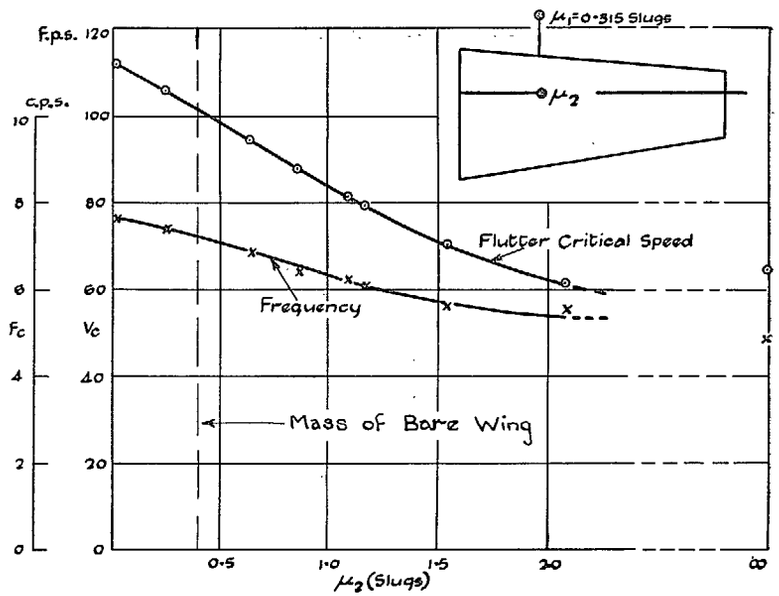

FIG. 9.

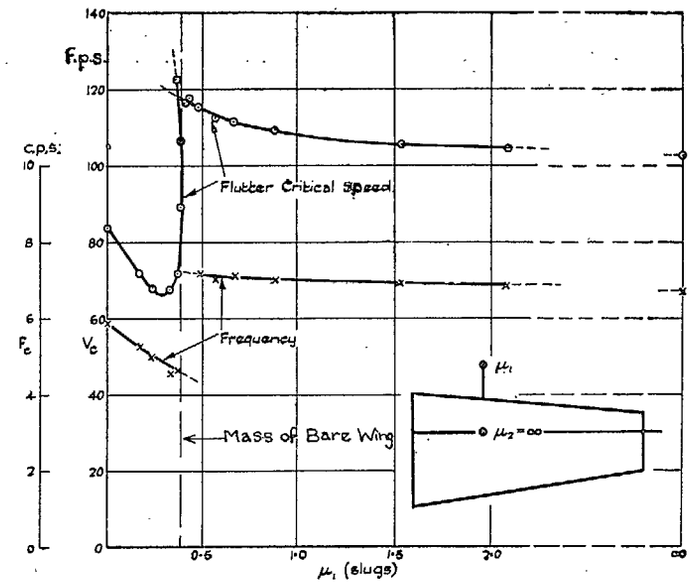

FIG. 11.

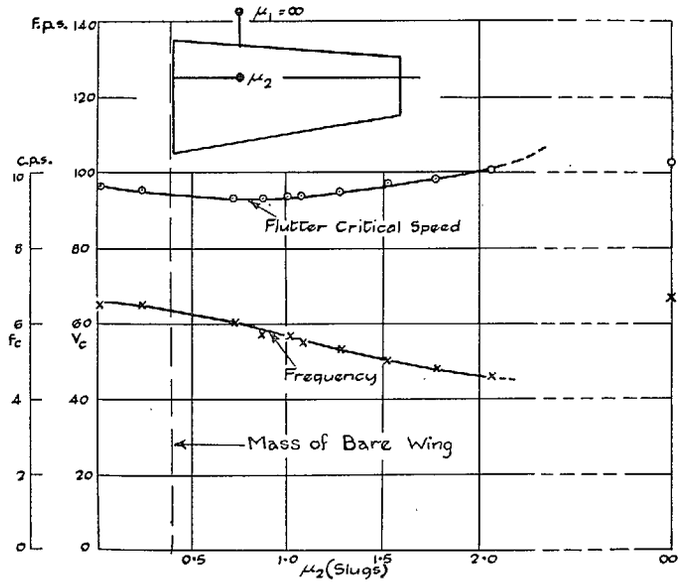

FIG. 10.

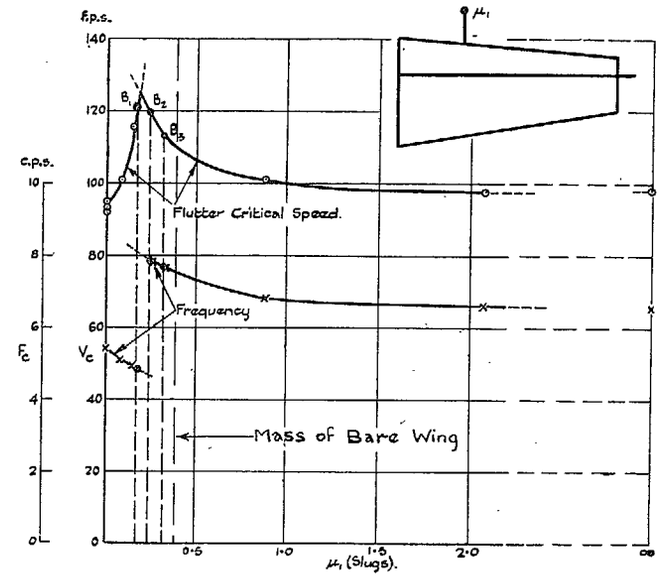

FIG. 12.

Variation of Critical Speed and Frequency with Mass Loading at $\eta = 0 \cdot 3$.

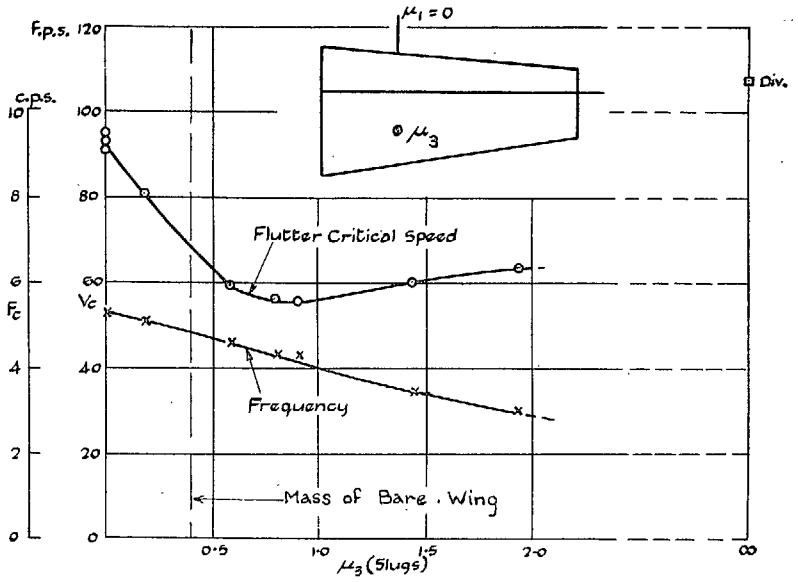

FIG. 13.

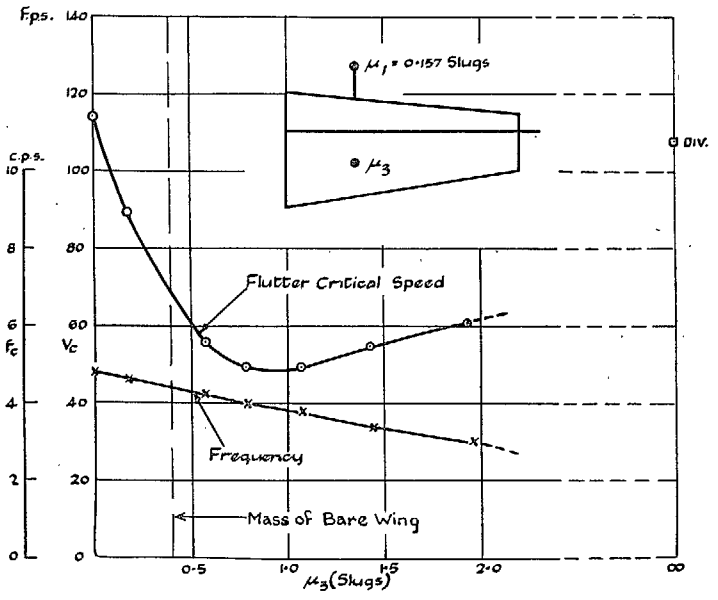

FIG. 14.

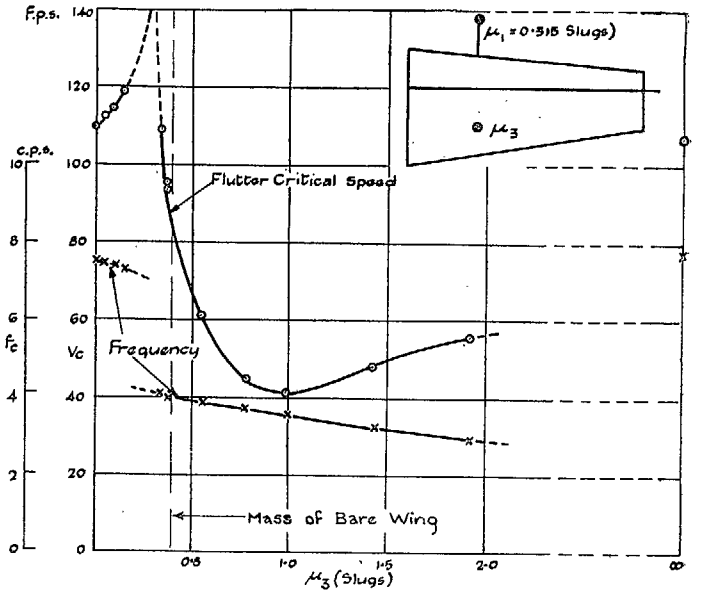

FIG. 15.

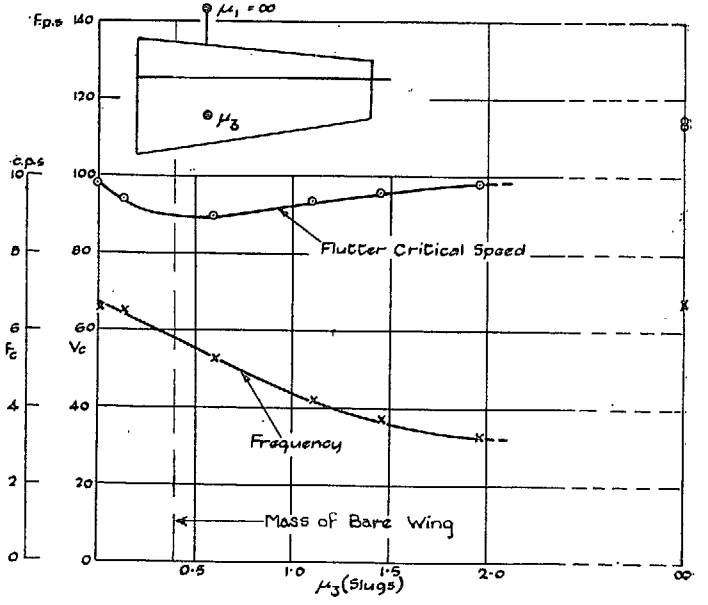

FIG. 16.

Variation of Critical Speed and Frequency with Mass Loading at $\eta = 0{\cdot}3$.

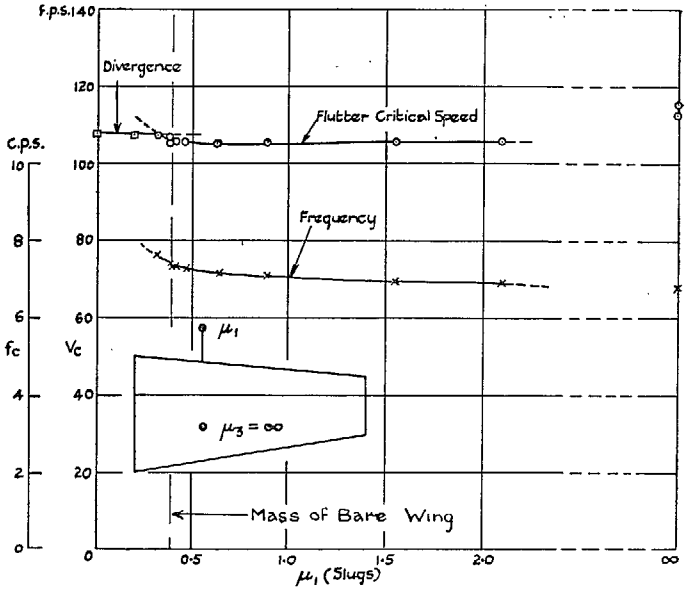

FIG. 17.

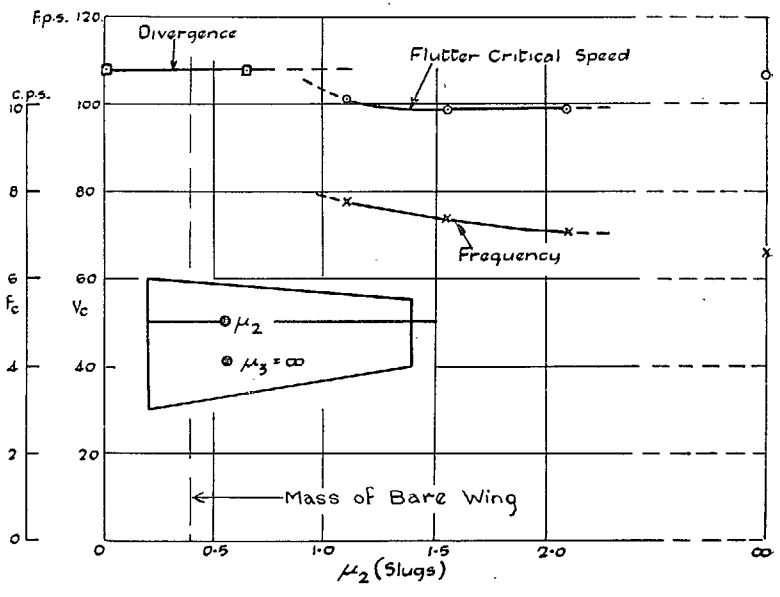

FIG. 19.

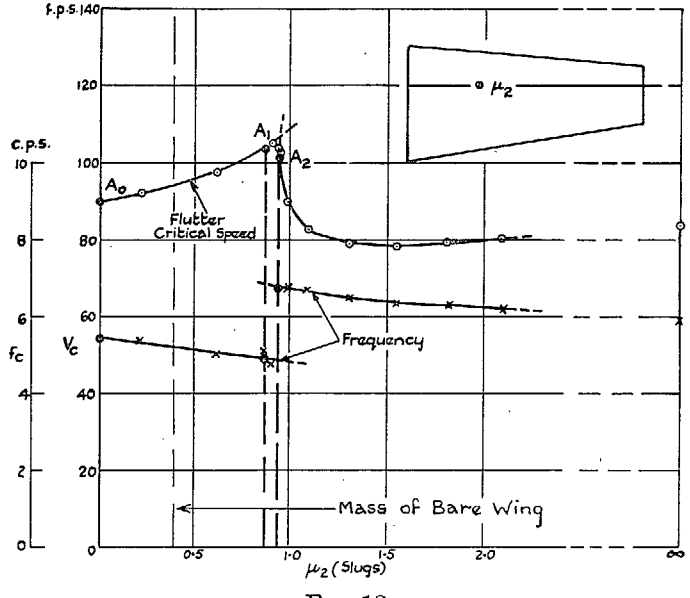

FIG. 18.

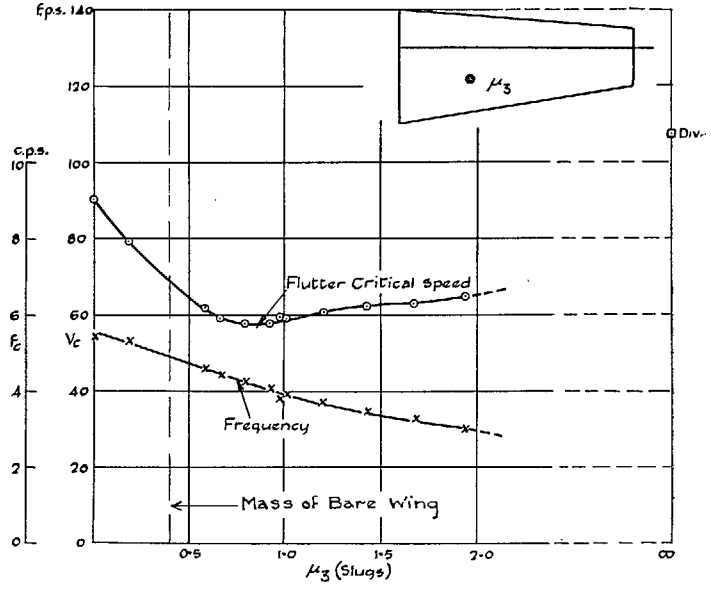

FIG. 20.

Variation of Critical Speed and Frequency with Mass Loading at $\eta = 0{\cdot}3$.

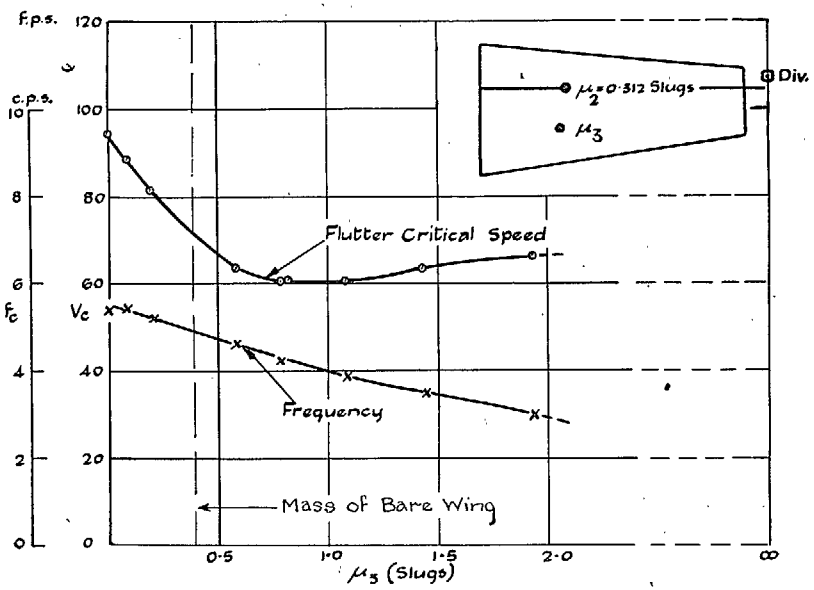

FIG. 21.

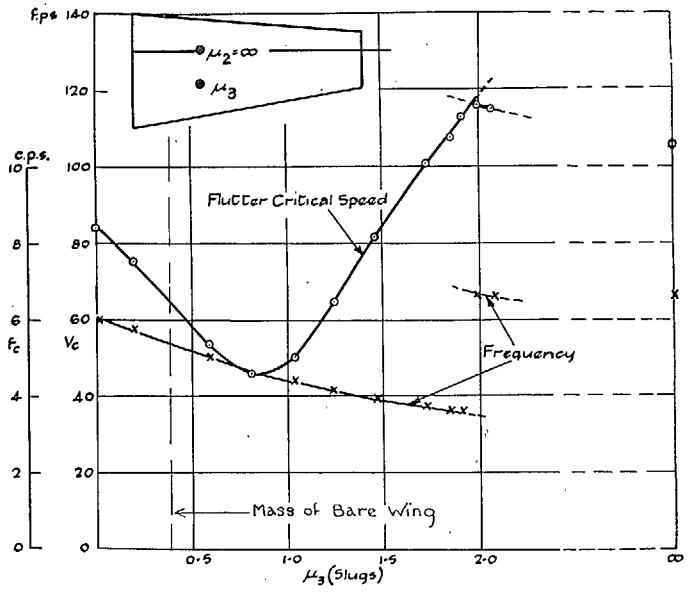

FIG. 22.

Variation of Critical Speed and Frequency with Mass Loading at $\eta = 0{\cdot}3$.

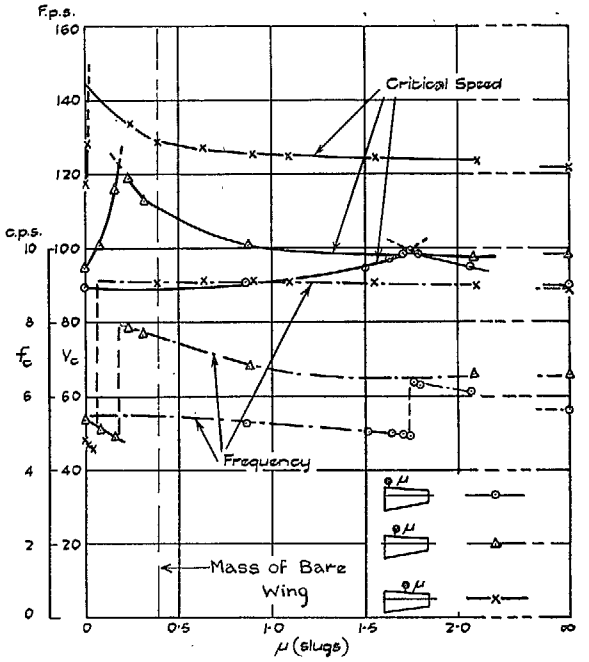

FIG. 23. Variation of Critical Speed and Frequency with Mass Loading forward of Leading Edge at $\eta = 0{\cdot}1$, $0{\cdot}3$ and $0{\cdot}5$.

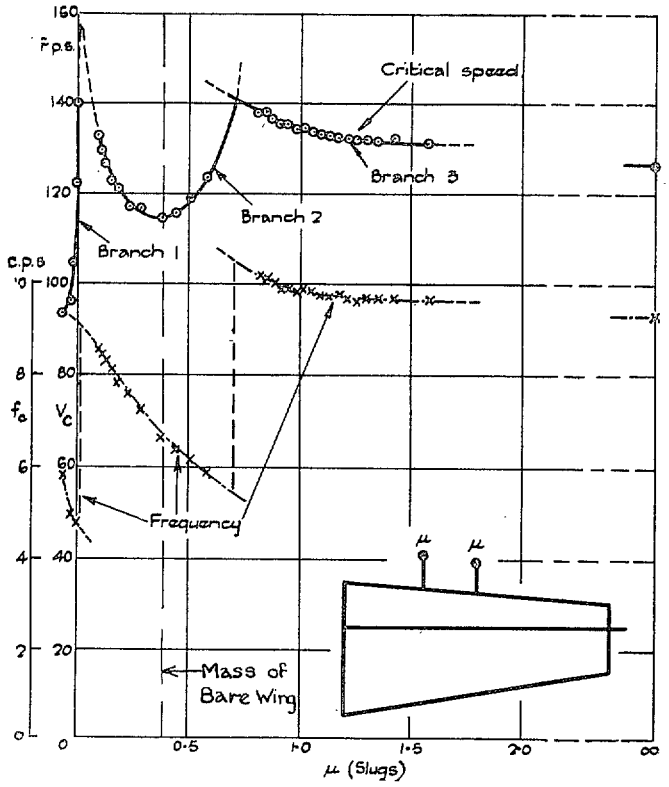

FIG. 24. Variation of Critical Speed and Frequency with Mass Loading forward of Leading Edge simultaneously at $\eta = 0{\cdot}3$ and $0{\cdot}5$.

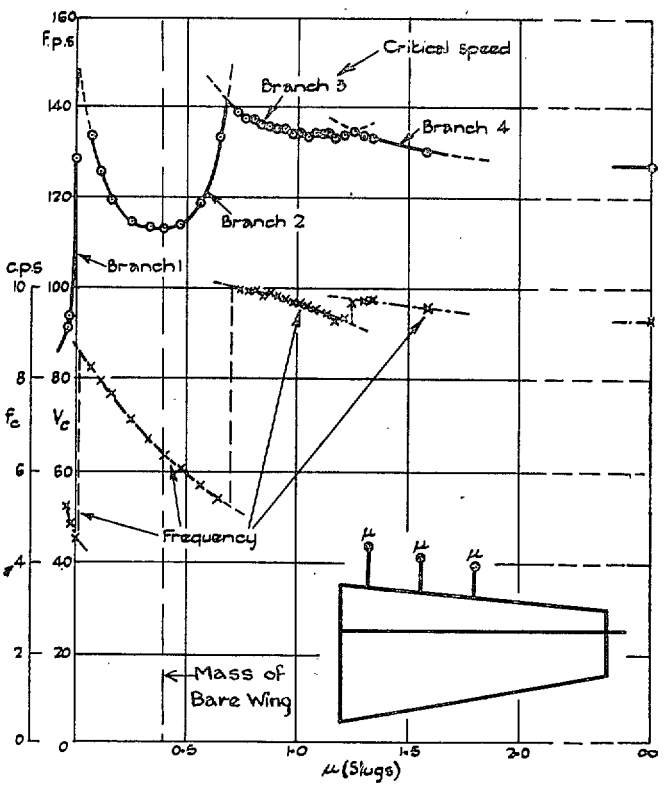

FIG. 25. Variation of Critical Speed and Frequency with Mass Loading forward of Leading Edge simultaneously at $\eta = 0{\cdot}1$, $0{\cdot}3$ and $0{\cdot}5$.

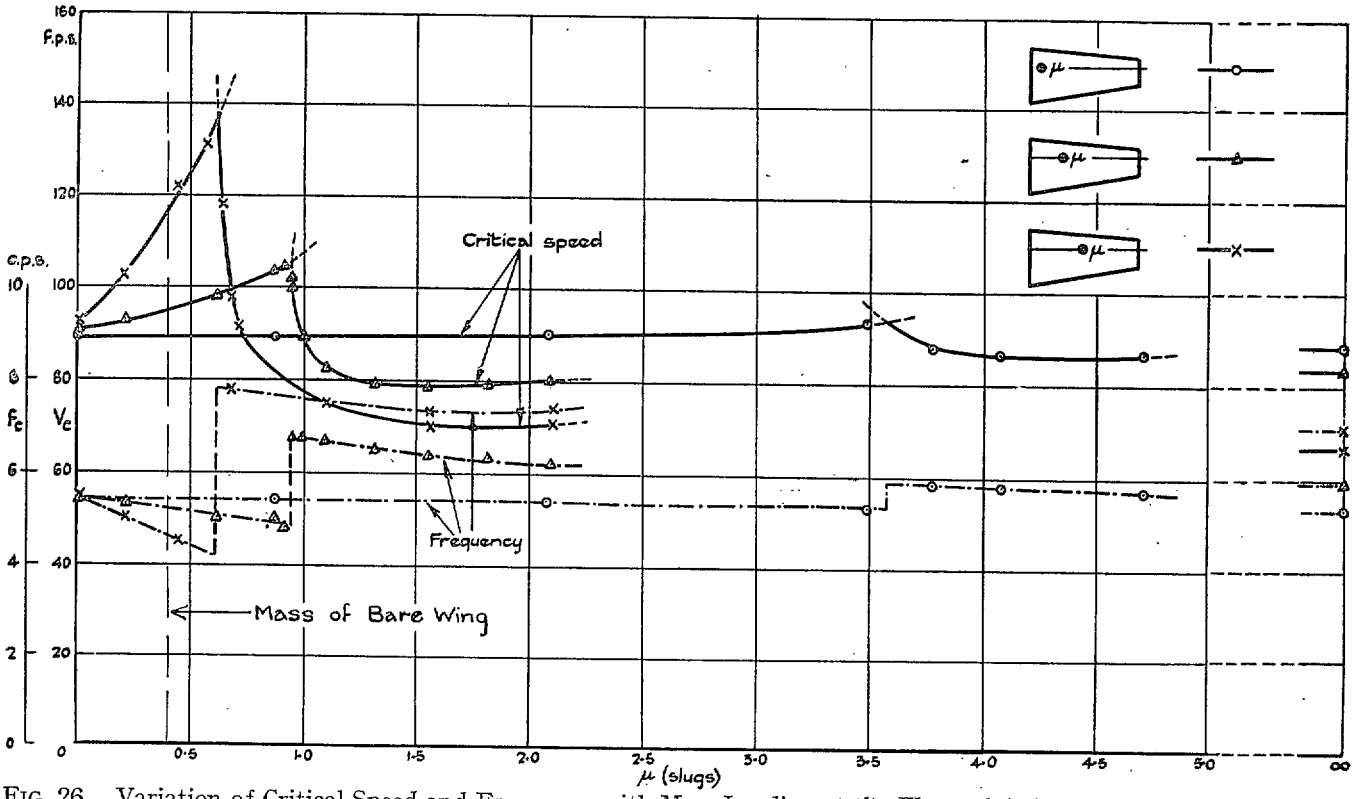

FIG. 26. Variation of Critical Speed and Frequency with Mass Loading at the Flexural Axis at $\eta = 0{\cdot}1$, $0{\cdot}3$ and $0{\cdot}5$.

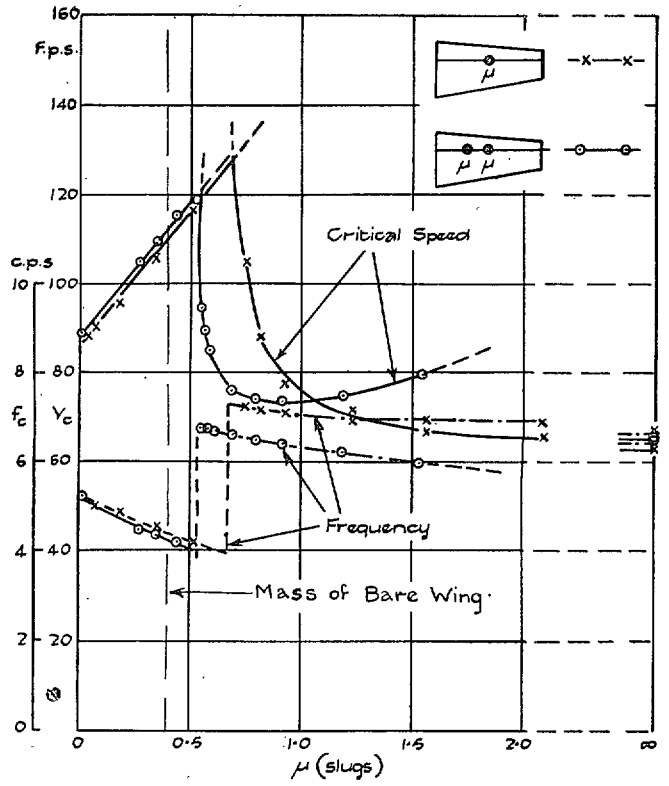

FIG. 27. Variation of Critical Speed and Frequency with Mass Loading at the Flexural Axis at $\eta = 0{\cdot}3$ and $0{\cdot}5$.

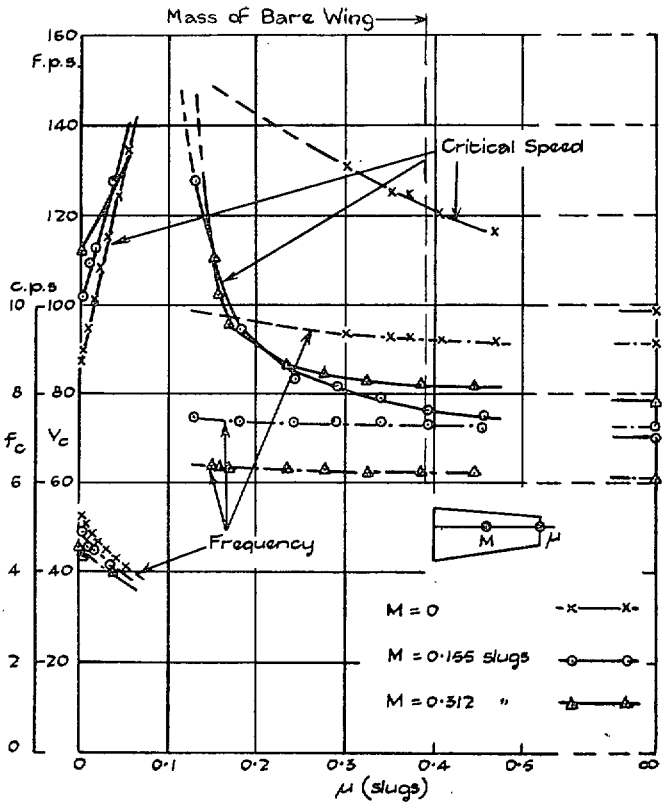

FIG. 28. Variation of Critical Speed and Frequency with Mass Loading at the Flexural Axis at $\eta = 0{\cdot}5$ and $1{\cdot}0$.

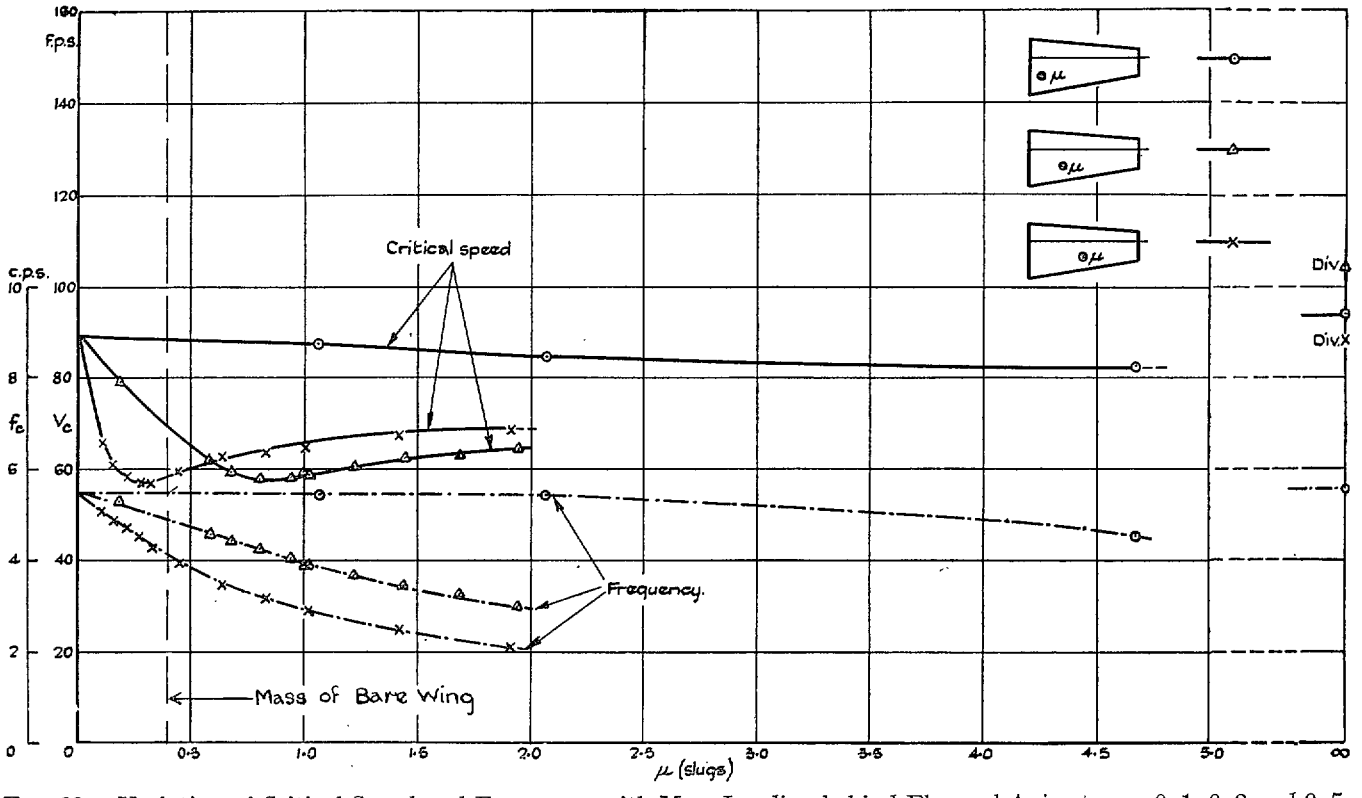

FIG. 29. Variation of Critical Speed and Frequency with Mass Loading behind Flexural Axis at $\eta = 0{\cdot}1$, $0{\cdot}3$ and $0{\cdot}5$.

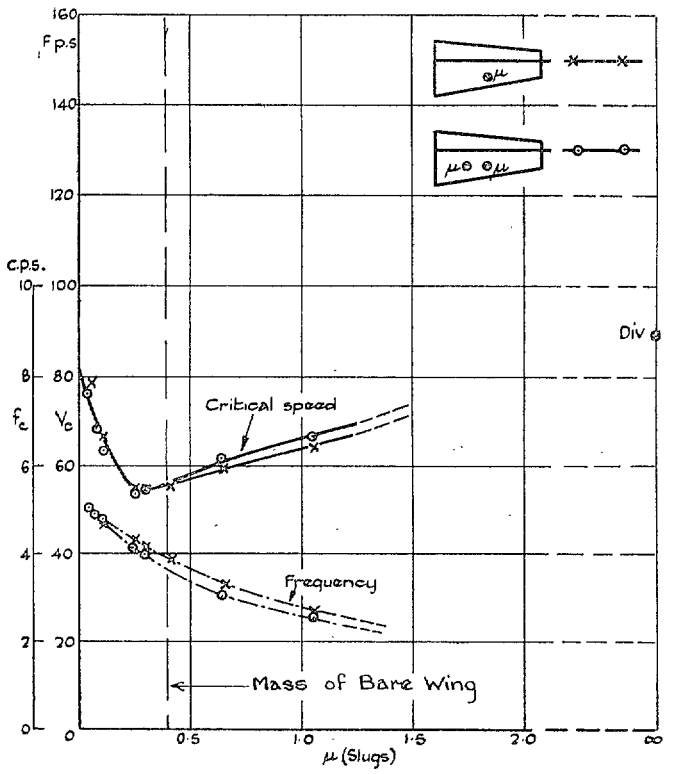

FIG. 30. Variation of Critical Speed and Frequency with Mass Loading behind Flexural Axis simultaneously at $\eta = 0{\cdot}3$ and $0{\cdot}5$.

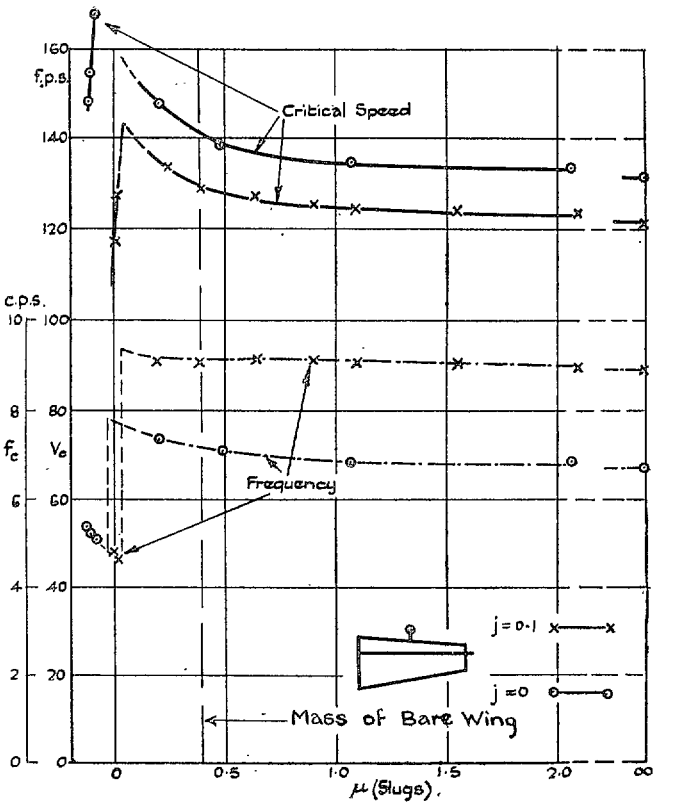

FIG. 31. Variation of Critical Speed and Frequency with Mass Loading forward of Leading Edge at $\eta = 0{\cdot}5$ for Two Positions of the Inertia Axis.

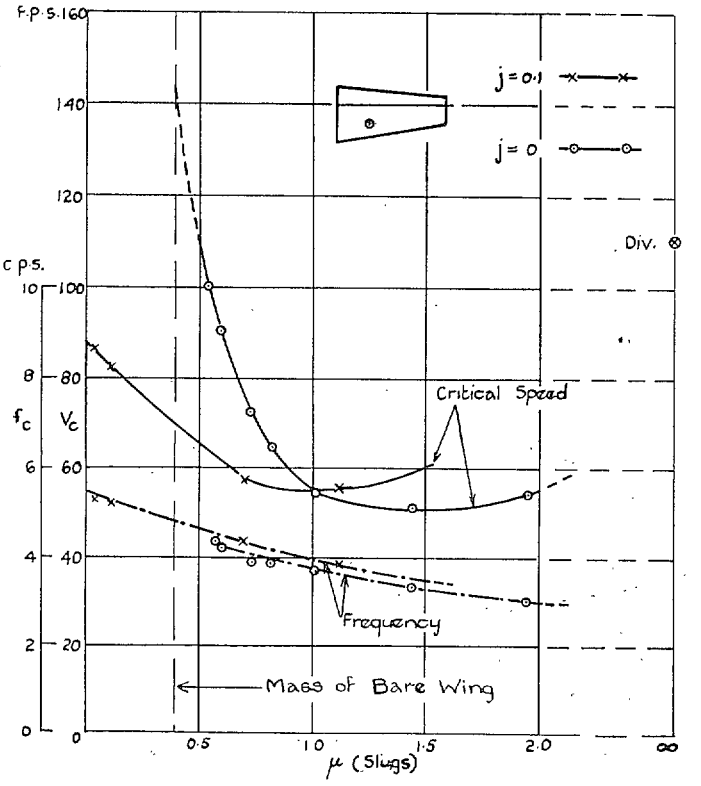

FIG. 32. Variation of Critical Speed and Frequency with Mass Loading behind the Flexural Axis at $\eta = 0{\cdot}3$ for Two Positions of the Inertia Axis.

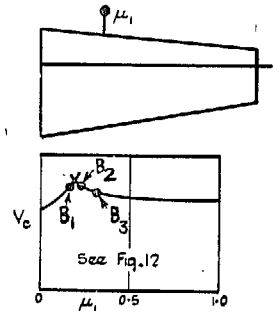

		Tip Amplitude Ratio Φ/Φ
⊙	Bare wing	0·232
×	B_1	0·410
△	B_2	0·103
⊡	B_3	0·101

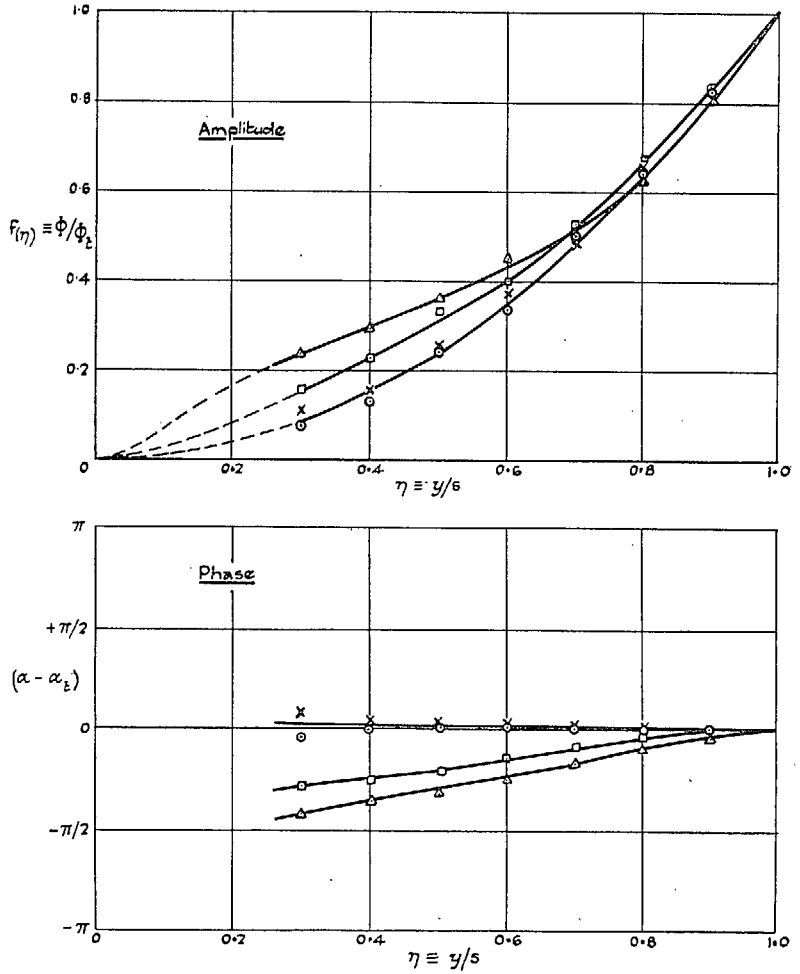

FIG. 33. Flexural Components.

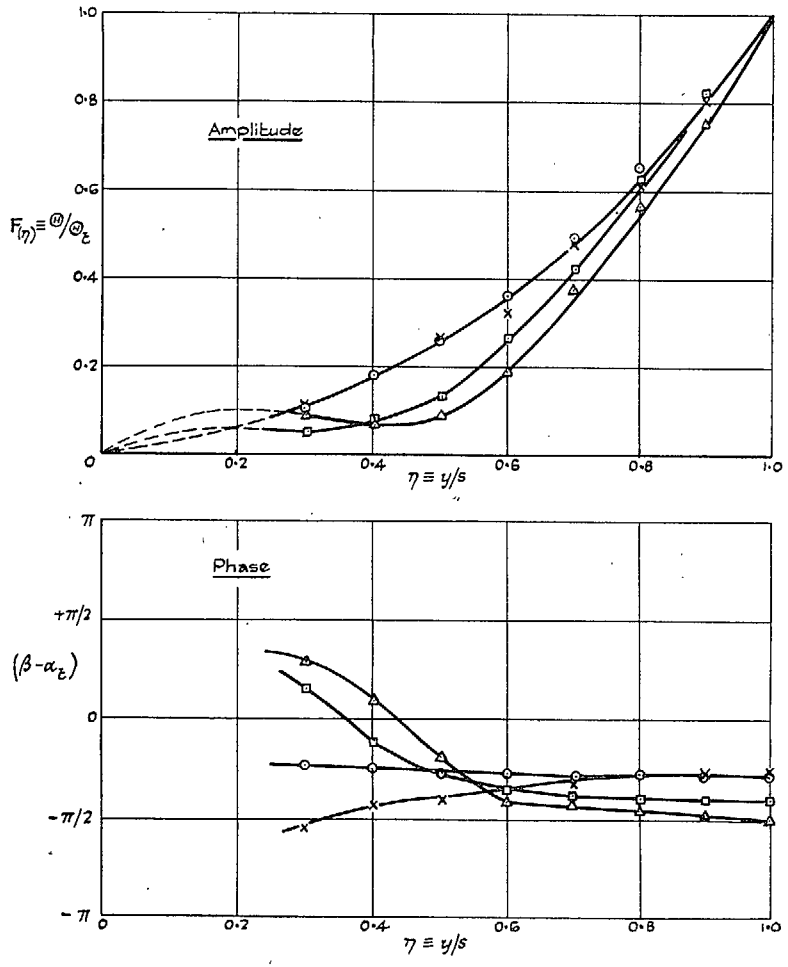

FIG. 34. Torsional Components.

Flutter Modes for some Conditions of Mass Loading forward of Leading Edge at $\eta = 0{\cdot}3$.

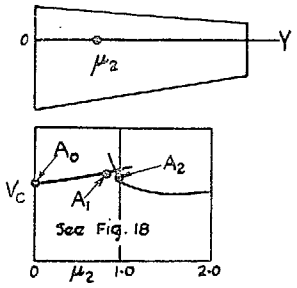

		Tip Amplitude Ratio $\bar{\Phi}/\Theta$
○	Bare wing, A_0	0·232
×	A_1	0·257
△	A_2	0·319

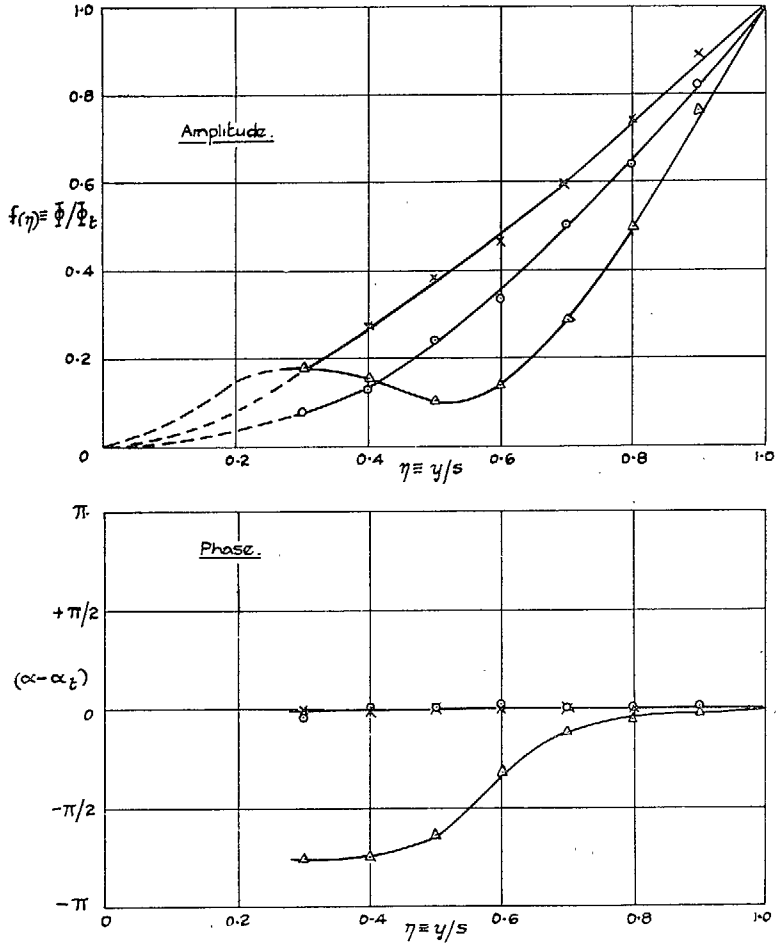

FIG. 35. Flexural Components.

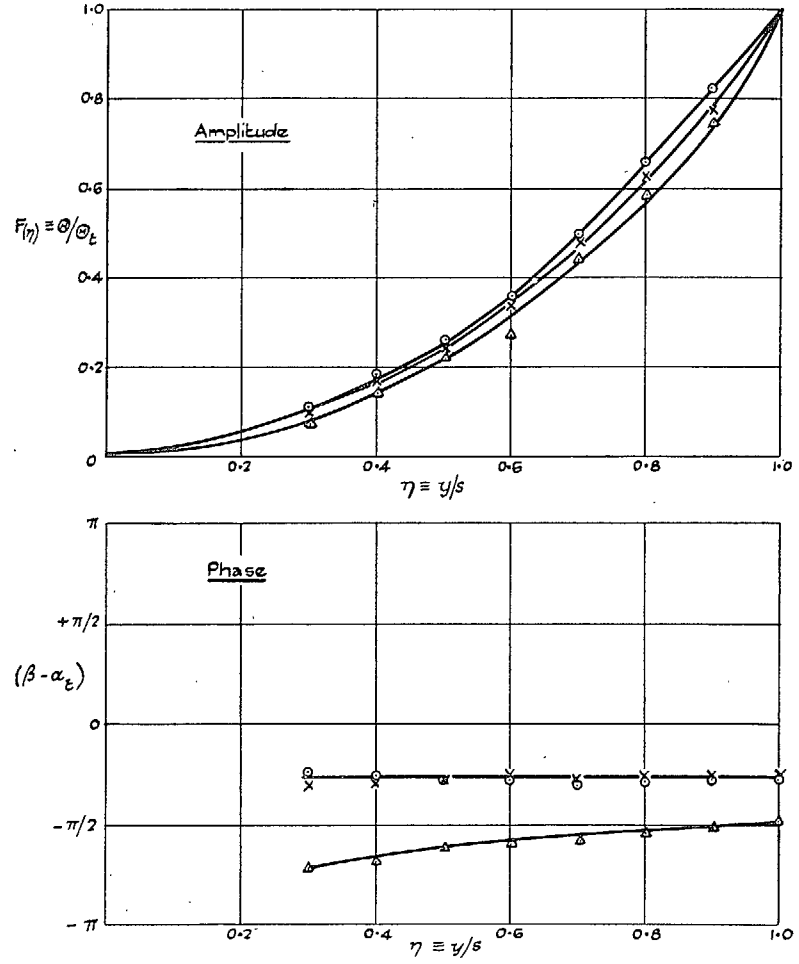

FIG. 36. Torsional Components.

Flutter Modes for some Conditions of Mass Loading at the Flexural Axis at $\eta = 0{\cdot}3$.

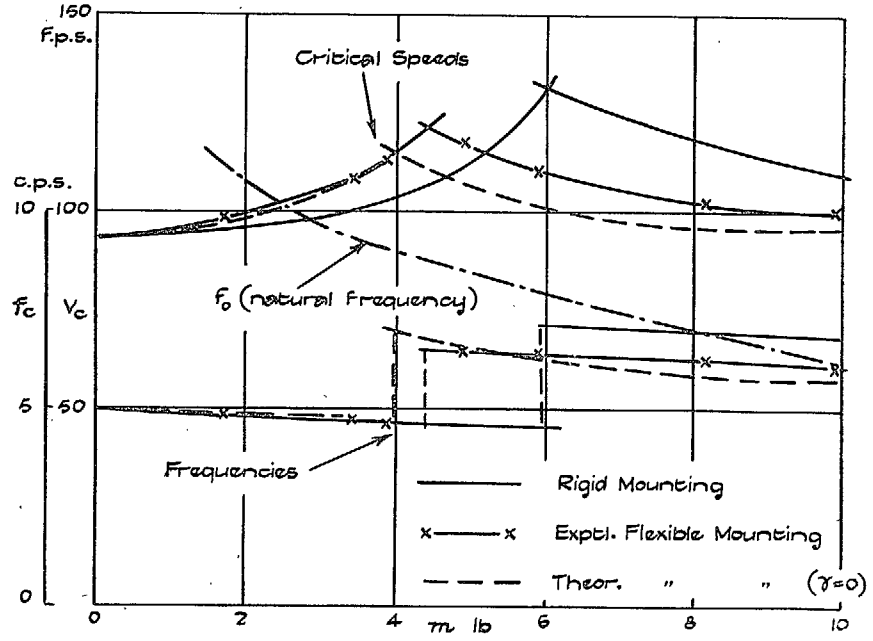

FIG. 37. Flexible Mounting Stiffness C_1 Relative Damping $\gamma = 0{\cdot}11$.

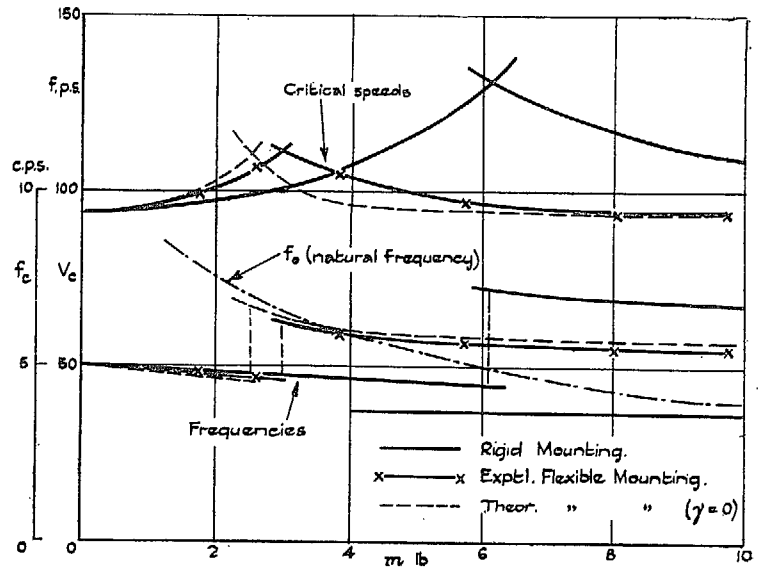

FIG. 38. Flexible Mounting. Stiffness C_2, Relative Damping $\gamma = 0{\cdot}10$.

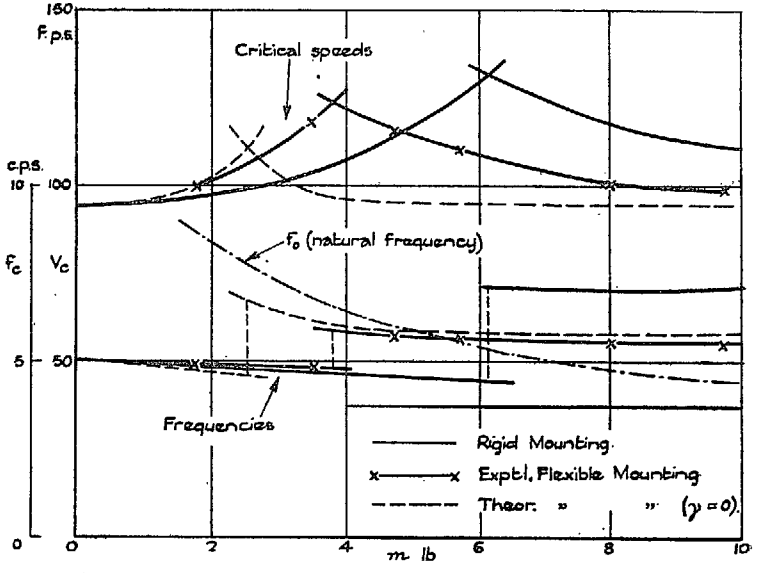

FIG. 39. Flexible Mounting. Stiffness C_2, Relative Damping $\gamma = 0{\cdot}34$.

Variation of Critical Speed and Frequency.

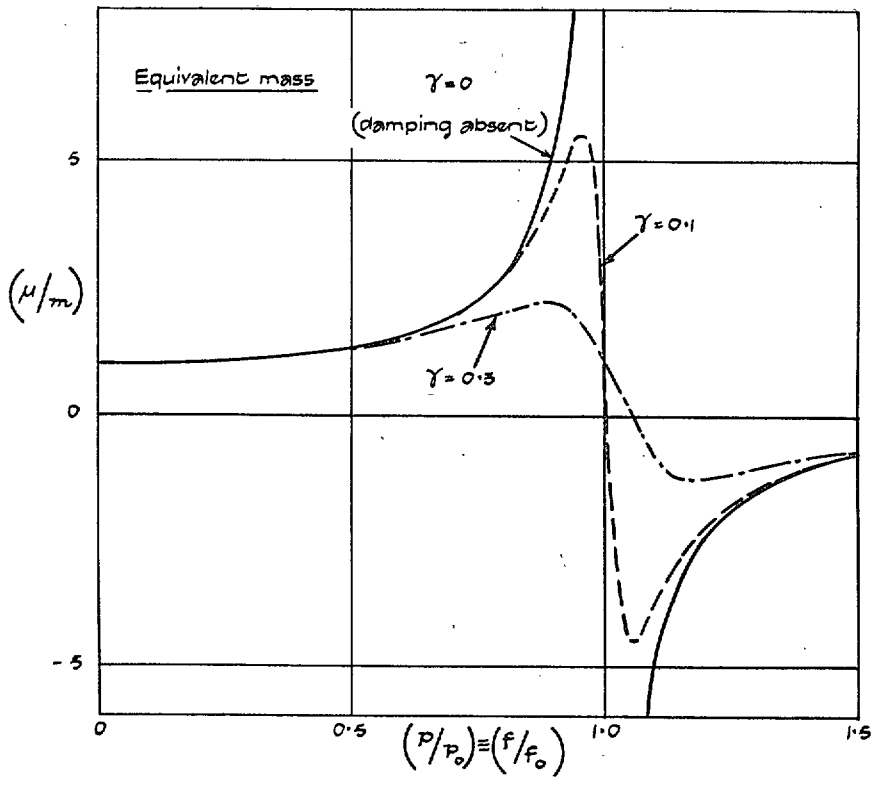

FIG. 40.

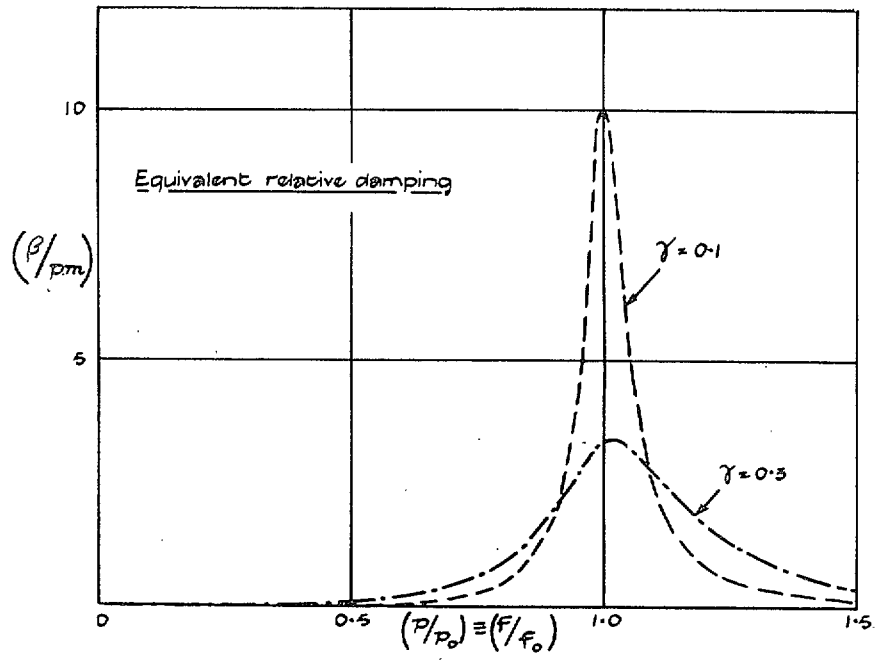

FIG. 41. Theoretical Equivalent Mass and Damping of Flexibly Supported Mass.

(92986) Wt. 13/806 K.5 4/51 Hw. PRINTED IN GREAT BRITAIN

Publications of the Aeronautical Research Committee

TECHNICAL REPORTS OF THE AERONAUTICAL RESEARCH COMMITTEE—

1934–35 Vol. I. Aerodynamics. 40*s.* (40*s.* 8*d.*)
Vol. II. Seaplanes, Structures, Engines, Materials, etc. 40*s.* (40*s.* 8*d.*)

1935–36 Vol. I. Aerodynamics. 30*s.* (30*s.* 7*d.*)
Vol. II. Structures, Flutter, Engines, Seaplanes, etc. 30*s.* (30*s.* 7*d.*)

1936 Vol. I. Aerodynamics General, Performance, Airscrews, Flutter and Spinning. 40*s.* (40*s.* 9*d.*)
Vol. II. Stability and Control, Structures, Seaplanes, Engines, etc. 50*s.* (50*s.* 10*d.*)

1937 Vol. I. Aerodynamics General, Performance, Airscrews, Flutter and Spinning. 40*s.* (40*s.* 9*d.*)
Vol. II. Stability and Control, Structures, Seaplanes, Engines, etc. 60*s.* (61*s.*)

1938 Vol. I. Aerodynamics General, Performance, Airscrews, 50*s.* (51*s.*)
Vol. II. Stability and Control, Flutter, Structures, Seaplanes, Wind Tunnels, Materials. 30*s.* (30*s.* 9*d.*)

1939 Vol. I. Aerodynamics General, Performance, Airscrews, Engines. 50*s.* (50*s.* 11*d.*)
Vol. II. Stability and Control, Flutter and Vibration, Instruments, Structures, Seaplanes, etc. 63*s.* (64*s.* 2*d.*)

ANNUAL REPORTS OF THE AERONAUTICAL RESEARCH COMMITTEE—

1933–34	1*s.* 6*d.* (1*s.* 8*d.*)
1934–35	1*s.* 6*d.* (1*s.* 8*d.*)
April 1, 1935 to December 31, 1936.	4*s.* (4*s.* 4*d.*)
1937	2*s.* (2*s.* 2*d.*)
1938	1*s.* 6*d.* (1*s.* 8*d.*)
1939-48	*In the press*

INDEXES TO THE TECHNICAL REPORTS OF THE ADVISORY COMMITTEE ON AERONAUTICS—

December 1, 1936 — June 30, 1939.	R. & M. No. 1850.	1*s.* 3*d.* (1*s.* 5*d.*)
July 1, 1939 — June 30, 1945.	R. & M. No. 1950.	1*s.* (1*s.* 2*d.*)
July 1, 1945 — June 30, 1946.	R. & M. No. 2050.	1*s.* (1*s.* 1*d.*)
July 1, 1946 — December 31, 1946.	R. & M. No. 2150.	1*s.* 3*d.* (1*s.* 4*d.*)
January 1, 1947 — June 30, 1947.	R. & M. No. 2250.	1*s.* 3*d.* (1*s.* 4*d.*)

Prices in brackets include postage.

Obtainable from

His Majesty's Stationery Office

York House, Kingsway, LONDON, W.C.2 429 Oxford Street, LONDON, W.1
P.O. Box 569, LONDON, S.E.1
13a Castle Street, EDINBURGH, 2 1 St. Andrew's Crescent, CARDIFF
39 King Street, MANCHESTER, 2 Tower Lane, BRISTOL, 1
2 Edmund Street, BIRMINGHAM, 3 80 Chichester Street, BELFAST

or through any bookseller.